



THEORETICAL STUDIES OF ACOUSTIC INTERACTION WITH THE
OCEAN BOTTOM AT LOW FREQUENCY

A DISSERTATION SUBMITTED TO THE GRADUATE DIVISION OF THE
UNIVERSITY OF HAWAII IN PARTIAL FULFILLMENT
OF THE REQUIREMENTS FOR THE DEGREE OF

DOCTOR OF PHILOSOPHY

IN GEOLOGY AND GEOPHYSICS

MAY 1980

By

Gerard John Fryer

Dissertation Committee:

George H. Sutton, Chairman
Joseph F. Gettrust
Murli H. Manghnani
Seymour O. Schlanger
Peter N. Dobson

We certify that we have read this dissertation and that in our opinion it is satisfactory in scope and quality as a dissertation for the degree of Doctor of Philosophy in Geology and Geophysics.

DISSERTATION COMMITTEE

Chairman

ACKNOWLEDGMENTS

Mark Odegard was primarily responsible for my becoming a seismologist and for my embarking on this work. Over the years he has been extremely generous with his time and I have benefited greatly from his scientific knowledge. I am grateful for his generous encouragement and guidance.

I wish to thank my committee for their forbearance and support; George Sutton and Joseph Gettrust in particular have been especially helpful. Brief conversations with Neil Frazer and Michael McKisic have proved more valuable than either of these gentlemen realise. I am also grateful to Dr. McKisic for providing the final needling necessary to get me to complete this work.

This research was supported by the Ocean Science and Technology Division of the Office of Naval Research.

ABSTRACT

The very high compressional and shear velocity gradients of marine sediments result in continuous interconversion between P and S types of motion at modestly low frequencies. Since the ray theories commonly used in modeling acoustic interaction with the ocean bottom implicitly assume that P and S are decoupled, the importance of such phenomena must be assessed. The problem is addressed here through investigation of the ocean-bottom reflectivity function.

The only practical approach for including all wave phenomena in a determination of reflectivities involves numerical solution of the wave equation. For a depth-varying structure the most efficient numerical scheme is the classical approximation by homogeneous layers. Unfortunately, the results of this analysis are so difficult to interpret that the physics of the reflection process is obscured. Some insight can be gained by transforming the frequency dependence of the reflectivity function to a time dependence. The resulting function (the plane-wave response) is amenable to physical interpretation and may be used as the basis for computing synthetic seismograms.

By assuming P and S wave potentials are independent and studying the effects of this on the reflectivity, the importance of gradient-driven coupling can be readily determined. For any realistic structure the coupling is small and can be ignored above 1 Hz.

TABLE OF CONTENTS

ACKNOWLEDGMENTS	iii
ABSTRACT	iv
LIST OF TABLES	vi
LIST OF ILLUSTRATIONS	vii
I. INTRODUCTION	1
II. MATHEMATICAL PRELIMINARIES	5
A. The Propagator	5
B. Reflectivity	8
III. THE INTEGRATION	13
A. Product Integration	13
B. Numerical Instabilities	16
C. Perturbing the Solution	19
D. A Comparison of Codes	22
E. Adaptive Methods	27
IV. GRADIENT-DRIVEN P-SV COUPLING.	29
V. RESULTS	
A. Model 1	31
B. Model 2	51
VI. DISCUSSION AND CONCLUSIONS	61
REFERENCES	64
APPENDIX A	
Reflectivity of the Ocean Bottom at Low Frequency	68
APPENDIX B	
A Slowness Approach to the Reflectivity Method of Seismogram Synthesis.	77

LIST OF TABLES

Table		Page
I	Test structure with high gradients	25
II	Model Parameters	33

LIST OF ILLUSTRATIONS

Figure		Page
1	Geometry of the problem considered	11
2	Comparison of Thomson-Haskell and Runge-Kutta reflectivity estimates	24
3	Parameters of Model 1	32
4	Modulus of the reflectivity function for Model 1 . . .	34
5	Shear propagation effects for Model 1	36
6	Error in the magnitude of the decoupled reflectivity for Model 1	38
7	Error in the phase of the decoupled reflectivity for Model 1	39
8	Comparison of complete and decoupled reflectivities for Model 1 at 10° incidence	41
9	Comparison of complete and decoupled reflectivities for Model 1 at 30° incidence	42
10	Comparison of complete and decoupled reflectivities for Model 1 at 50° incidence	43
11	Comparison of complete and decoupled reflectivities for Model 1 at 70° incidence	44
12	Synthetic pressure records for Model 1	48
13	A ray interpretation of Figure 12	49
14	Modulus of the reflectivity function for Model 2 . . .	53
15	Error in the magnitude of the decoupled reflectivity for Model 2	54
16	Error in the phase of the decoupled reflectivity for Model 2	55
17	Magnitude error for Model 2 if only 120m of sediments are included	58
18	Phase error for Model 2 if only 120m of sediments are included	59

I. INTRODUCTION

The nature of the interaction of acoustic waves with the ocean bottom is profoundly different at low and high frequencies. For the large angles of incidence (i.e. small grazing angles) appropriate in long range propagation problems, the high-frequency response of the bottom can be very well explained using geometrical ray theory and treating the ocean bottom as a fluid (Mitchell and Lemmon, 1979). This fluid model is no longer adequate if energy penetrating the bottom impinges on the sediment-basement interface as conversion of compressional waves to shear waves then becomes important. Even for rays bottoming within the sedimentary sequence such interaction will occur unless the sequence is thick compared to the wavelength. If interaction occurs then the bottom must be modeled as an elastic medium. Even when shear conversion is important, the shear disturbance arises from energy partition at interfaces so again ray theory (or strictly, a high-frequency asymptotic solution to the wave equation) would be capable of explaining the response. At low frequencies however, ray theory breaks down in media with strong velocity gradients such as marine sediments. At sufficiently low frequency, zones of velocity gradient appear similar to first-order discontinuities, so partial reflections occur (Chapman, 1980). Vidmar and Foreman (1979) estimate that for marine sediments such effects can be neglected above 10 Hz. However at the large angles of incidence of interest in long range propagation problems, such partial reflections can probably be completely ignored at all frequencies as they would be

indistinguishable from the classical ray theory refractions. A more important wave phenomenon occurs at lower frequencies: The fundamental ray concept of separate compressional (P) and shear (S) propagation then becomes inappropriate as the P and S motions are intrinsically coupled. Upward refraction of seismic energy then leads to continuous interconversion between P and S types of motion. This coupling would be greatest when energy reaches turnover depth high in the sedimentary column where the velocity gradients are the greatest. It is therefore of potential importance in long-range propagation. Following Richards' (1974) scheme for computing the coupling coefficients, Vidmar and Foreman (1979) estimated that this effect should be expected in marine sediments at frequencies up to 3 Hz. The nature and consequences of this coupling on the reflectivity characteristics of the ocean bottom have been inadequately described and are the primary topic of this paper.

The interaction of acoustic energy with a vertically heterogeneous ocean bottom is conveniently described in frequency-wavenumber space by the reflectivity function, which, because of its wavenumber dependence, is also termed the plane wave reflection coefficient. In any practical application the computed reflectivity function is compared with observations in some manner or used to make predictions of bottom loss. In either case the transformations from frequency-wavenumber to time-distance space must ultimately be performed. Such transformations are fundamental in the computation of synthetic seismograms (Chapman, 1978) and are necessary to explain the phenomenon of "negative bottom loss" (Santaniello, et

al., 1979). The necessity to perform transformations means that knowing the reflectivity at one point in ω - k space is then of little value; for the transforms to be evaluated the reflectivity must be known over a finite area. Since reflectivity values are computed at discrete points in ω - k , the need to sample areally means that numerous computations must be made, with a sampling density adequate to define the true surface accurately. These repetitive computations mean that determination of the reflectivity function is an inherently expensive proposition so efficient means of performing the computation is highly desirable.

The reflectivity function is obtained from the solution of the wave equation. Only one analytic solution to the wave equation for heterogeneous media has been presented so far and this is valid only for the case when compressional and shear velocity gradients are identical (Gupta, 1966a). This property is not exhibited by marine sediments (Hamilton, 1979b) so some approximate solution must be found. The wave equation can always be solved by direct numerical integration but all numerical integration procedures suffer the same disadvantages: they are numerically expensive and offer little insight into the reflection process. By contrast, asymptotic solutions use about an order of magnitude less computation time and are more amenable to physical interpretation. For elastic media appropriate asymptotic solutions are the WKBJ approximation (Richards, 1971), or where that is invalid, the Langer approximation (Chapman, 1974; Richards, 1976). However, because these are high-frequency approximations they are in essence ray theory methods and are

incapable of handling gradient-driven P-S coupling. Low-frequency asymptotic expansions are also possible (Molotkov et al., 1976), but these are inconvenient to use in marine acoustics where the primary interest is in moderately low to high frequencies. Recently Chapman (1980) has proposed an iterative scheme based on the Langer approximation which can apparently accommodate both partial reflections and P-S coupling. This method is not quite of general application as it can accept only single turning points, and it is not clear how attenuative effects can be included, but it looks extremely promising.

In the absence of acceptable analytic or asymptotic solutions to the wave equation it is necessary to resort to direct numerical integration. Only numerical integration can at present provide complete solutions (including P-S coupling effects) and handle arbitrary depth and frequency dependent variation of elastic parameters. This paper presents a comparison of some of the numerical integration procedures and describes how these can be used to assess the importance of gradient-driven P-S coupling. The goal of this work was to determine the most efficient means of computing ocean bottom reflectivity at low frequency and to define what is meant by "low frequency" so that the realm of applicability of the more efficient asymptotic solutions could be mapped.

II. MATHEMATICAL PRELIMINARIES

We shall consider motion in a stratified isotropic elastic halfspace whose density ρ and Lamé parameters, λ and μ , are functions of depth only. Acoustic waves in a fluid overlying the halfspace will excite only P-SV motion; horizontally polarized shear motion can be ignored. Without loss of generality the coordinate system can be defined so that all stresses and displacements are independent of the y-coordinate.

A. The Propagator

The general boundary condition on any wave propagation is that the horizontal and vertical displacements, u and w , and the normal and tangential stresses, σ_{zz} and σ_{zx} , be continuous across any horizontal plane. To reduce the problem to one in the z coordinate only, we consider the behaviour of the double Fourier transformed stress-displacement vector

$$s(k, \omega, z) = (\bar{u}, \bar{w}, \bar{\sigma}_{zz}, \bar{\sigma}_{zx})^T$$

$$= \int_{-\infty}^{\infty} \int_{-\infty}^{\infty} (u, w, \sigma_{zz}, \sigma_{zx})^T \exp[i(\omega t - kx)] dx dt,$$

where the superscript T denotes a transpose. For convenience in the following discussion we drop the arguments k and ω ; they are to be understood implicitly for all matrices.

By double Fourier transform of the constitutive equation and the wave equation it is straightforward to show that the behaviour of s is described by the differential system

$$\frac{d}{dz} s(z) = A(z)s(z) \quad (1)$$

in which the coefficient matrix is

$$A(z) = \begin{pmatrix} 0 & -ik & 0 & (\beta^2 \rho)^{-1} \\ -ik(1-2\beta^2/\alpha^2) & 0 & (\alpha^2 \rho)^{-1} & 0 \\ 0 & -\rho\omega^2 & 0 & -ik \\ 4k^2\beta^2\rho(1-\beta^2/\alpha^2)-\rho\omega^2 & 0 & -ik(1-2\alpha^2/\beta^2) & 0 \end{pmatrix} \quad (2)$$

(Gilbert and Backus, 1966). Here we have defined

$$\alpha^2 = (\lambda + \mu)/\rho; \quad \beta^2 = \mu/\rho.$$

In a homogeneous medium, α and β may be identified as the compressional and shear wave speeds.

The propagator or matricant of the system of equations (1) is the

unique continuous solution of the matrix equation

$$\frac{d}{dz} P(z, z_1) = A(z) P(z, z_1),$$

(3)

$$P(z_1, z_1) = I$$

(Gilbert and Backus, 1966), where I is the identity and z_1 is some reference depth.

It is a consequence of the uniqueness theorem that if the specific boundary condition applied at z_1 is $s(z_1)$, then the response vector at z is

$$s(z) = P(z, z_1) s(z_1).$$

Hence the term "propagator." If the system matrix A is constant, then obviously

$$P(z, z_1) = \exp[(z-z_1) A].$$

Even when A is not constant, the solution for $P(z, z_1)$ has exponential-like properties, in particular

$$P(z, z_1) = P(z, z_r) P(z_r, z_1) \tag{4}$$

(Pease, 1965, p. 175-176). The importance of these properties will become apparent later.

B. Reflectivity

To determine reflectivities it is necessary to relate the stress-displacement vector to the elastic wave field. To do this we make the transformation

$$s = T\phi \quad (5)$$

(Dunkin, 1965) where T is the eigenvector matrix for A so that

$$T^{-1}AT = \Lambda$$

where Λ is diagonal. The vector ϕ satisfies the equation

$$\frac{d\phi}{dz} = H(z)\phi \quad (6)$$

where

$$H(z) = \Lambda - T^{-1}dT/dz$$

(Kennett et al, 1978). If the system matrix $H(z)$ satisfies the Lipschitz condition then the solution of the system (6) is

$$\Phi(z) = E(z, z_1) \Phi(z_1)$$

where $E(z, z_1)$ is the propagator of the system. If the medium is homogeneous then T is independent of z so that $H = \Lambda$. The potential propagator E is then given by

$$E(z, z_1) = \exp[(z-z_1)\Lambda]. \quad (7)$$

The diagonal entries of Λ are the eigenvalues of A , so for a homogeneous medium

$$\Lambda = \text{diag}(-iv_\alpha, -iv_\beta, iv_\alpha, iv_\beta)$$

where v_α, v_β are the vertical wavenumbers for P and S propagation,

$$v_\alpha^2 = \omega^2/\alpha^2 - k^2,$$

$$v_\beta^2 = \omega^2/\alpha^2 - k^2,$$

with

$$\text{Im } v_\alpha, v_\beta \geq 0.$$

In the homogeneous case the elements of Φ can be identified as up and downgoing P and SV potentials (Kennett et al, 1978), so

$$\Phi = (\phi^U, \psi^U, \phi^D, \psi^D)^T \quad (8)$$

where ϕ, ψ represent the P and SV potentials and superscripts U, D represent upgoing and downgoing waves.

We now consider the ocean bottom structure shown schematically in Figure 1. The structure consists of a homogeneous ocean above depth $z=z_1$, a homogeneous basement below $z=z_n$, and a sediment layer between these two depths. Within the sediments the elastic parameters may vary in an arbitrary manner. We use subscripts 0 and n to refer to the fluid and elastic halfspaces respectively (this scheme anticipates the later layered approximation). The wave potentials ϕ_0 and ϕ_n in the ocean and basement are related by

$$\Phi_n(z_n) = M\Phi_0(z_1) + Bs'$$

(Fryer, 1978, Appendix A), where

$$B = T_n^{-1}P(z_n, z_1),$$

$$M = BT_0$$

and

$$s' = (\bar{u}(z), 0, 0, 0)^T.$$

Here T_0 and T_n are the eigenvector matrices for the upper and lower

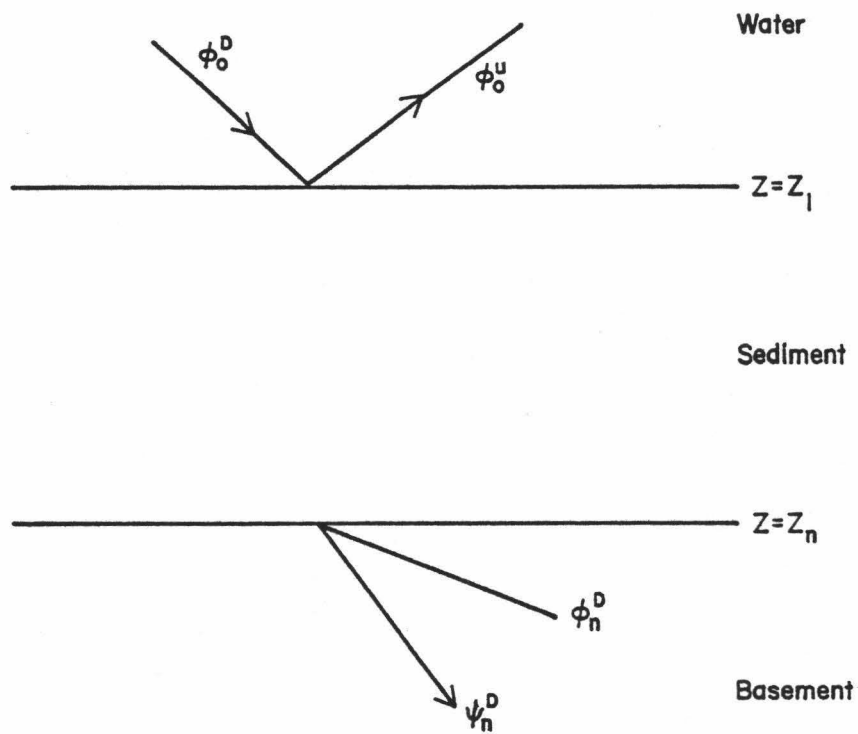


Figure 1. Geometry of the problem considered: an elastic sedimentary sequence sandwiched between fluid and elastic halfspaces.

halfspaces; since the halfspaces are homogeneous these matrices are independent of depth. The plane wave reflectivity of the ocean bottom, R , is given by

$$R = \phi_0^U(z_1) / \phi_0^D(z_1) = (b_{21}m_{13} - b_{11}m_{23}) / (b_{11}m_{21} - b_{21}m_{11}) \quad (9)$$

(Fryer, 1978), where b_{ij} , m_{ij} are the ij elements of B and M .

III. THE INTEGRATION

To compute reflectivities the fundamental problem is to find the stress propagator $P(z_n, z_1)$ of equation (3). As described in the introduction, we choose to solve equations (3) by numerical integration so that an arbitrary depth variation of elastic properties can be accommodated.

A. Product Integration

One of the most straightforward and conceptually simple integration procedures for numerical integration of a differential system is the product integral method of Volterra (1887; Gilbert and Backus, 1966). The interval from z_1 to z_n can be subdivided into a sequence of sections

$$z_1 < z_2 < z_3 \dots < z_{n-1} < z_n.$$

From equation (4) the propagator for the whole interval is the product of the subinterval propagators

$$P(z_n, z_1) = P(z_n, z_{n-1})P(z_{n-1}, z_{n-2}) \dots P(z_2, z_1). \quad (10)$$

The subintervals should be chosen so that within each $A(z)$ is essentially constant, i.e., if

$$A(z) = A_k + C(z), \quad z_k \leq z \leq z_{k+1}, \quad (11)$$

where A_k is constant, then $C(z)$ should be small. A reasonable choice of the "average" system matrix for the subinterval is

$$A_k = A(\zeta_k),$$

where

$$\zeta_k = (z_k + z_{k+1})/2.$$

The stress propagator for a homogeneous layer is the solution of

$$\frac{d}{dz} D(z, z_k) = A_k D(z, z_k),$$

$$D(z_k, z_k) = I.$$

If $C(z)$ is small then the subinterval propagator is given approximately by

$$P(z_{k+1}, z_k) \approx D(z_{k+1}, z_k) = \exp(A_k \Delta z_k) \quad (12)$$

where

$$\Delta z_k = z_{k+1} - z_k.$$

Equation (12) can be expanded

$$D(z_{k+1}, z_k) \approx I + A_k \Delta z_k \quad (13)$$

so that, from equations (10) and (12),

$$P(z_n, z_1) \approx \prod_{k=1}^n (I + A_k \Delta z_k). \quad (14)$$

In the limit, as all $\Delta z_k \rightarrow 0$, equation (14) becomes the product integral of $A(z)$ and the expression becomes a true equality (Birchhoff, 1937).

In seismology it is not usual to use the approximate expansion (13), the desired propagator is simply obtained from equations (10) and (12). Rather than evaluating the exponential in equation (12) directly, it is simpler to use the transformation (5) and the potential propagator for the homogeneous case given in equation (7). If we write $T_k = T(\zeta_k)$, then the propagator for the homogeneous subinterval is given by

$$D_k = D(z_{k+1}, z_k) = T_k \exp(\Lambda_k \Delta z_k) T_k^{-1},$$

where Λ_k is computed using the velocities $\alpha(\zeta_k)$ and $\beta(\zeta_k)$. The desired propagator is then given by

$$P(z_n, z_1) \approx D_{n-1} D_{n-2} \dots D_2 D_1.$$

Physically, this procedure may be regarded as approximating the

structure by a series of thin homogeneous layers. This method was first used in seismology by Thomson (1950) and Haskell (1953) and is now known as the Thomson-Haskell method; the homogeneous subinterval propagators D_k are often referred to as Haskell layer matrices. The method has enjoyed considerable popularity and details of its application are widely available. A description which is particularly appropriate to the application of this paper is given by Fuchs (1968).

Because the Thomson-Haskell approach approximates a continuously varying structure with homogeneous layers, all conversions between P and S must be relegated to the interfaces between the layers. It is for this reason that there is a widespread suspicion that the method does not adequately handle P-S conversion phenomena caused by velocity gradients. However, convergence of the product integral technique has been demonstrated both theoretically (Birchoff, 1937) and numerically (Gupta, 1966b). This means that the Thomson-Haskell method does adequately treat P-S conversions if the layer thicknesses are made small enough.

B. Numerical instabilities

Unfortunately, the Thomson-Haskell method as just formulated is unstable at large wavenumbers. Evaluating expressions such as (9) then involves taking the difference between large and nearly equal quantities and severe loss of precision can result. Dunkin (1965)

gives an excellent explanation of how the instabilities arise and proves that they can be reduced by expanding the 4×4 matrices into the 6×6 matrices of all possible second-order subdeterminants. This approach has become known as the delta matrix method after a similar procedure used in the analysis of mechanical systems (Pestel and Leckie, 1963, p. 194-200). In computing reflectivities the delta matrix method has the advantage that only a single row need be carried through the matrix multiplications, so in addition to increased stability, considerable savings in computation time can be realised. Symmetries in the delta matrices mean that computation need be performed using only a reduced system of 5×5 matrices (Watson, 1970). The use of this reduced delta matrix method in computing reflectivities has been outlined by Kind (1976), and the method applied to ocean bottom reflectivity by Fryer (1978).

The Thomson-Haskell instability is not caused by any failure of the product integral approach, but is an inherent problem associated with the differential system (3). Any numerical scheme for integrating equation (3) directly will become unstable when trying to extend the propagator to depths below the P turning point, because of leakage of an exponentially growing P term into other parts of the solution (Chapman and Phinney, 1972). This instability is essentially the same as the problem encountered in "stiff" differential equations (Gear, 1971, p. 209-211), but is unusual in that it exists regardless of the direction of integration. This is because we are solving for the complete propagator, which describes both upgoing and downgoing disturbances. Dunkin's solution to the stability problem may be

applied directly to the original system; by replacing the system (3) by the equivalent sixth-order system the stability problem is greatly reduced (Gilbert and Backus, 1966; Chapman and Phinney, 1972). The reduction to fifth-order is possible because the system matrix for the sixth-order system has repeated eigenvalues. This means that it is possible to replace the original differential system (3) by

$$\frac{d\hat{P}}{dz} = \hat{A}\hat{P}, \quad (17)$$

where the 5 X 5 system matrix \hat{A} is given by

$$\hat{A}(z) = \begin{pmatrix} 0 & a_{23} & 0 & -a_{14} & 0 \\ a_{32} & 0 & 2a_{12} & 0 & -a_{14} \\ 0 & a_{21} & 0 & a_{12} & 0 \\ -a_{14} & 0 & 2a_{21} & 0 & a_{23} \\ 0 & -a_{14} & 0 & a_{32} & 0 \end{pmatrix}$$

Here a_{ij} represents the ij element of the original system matrix A (equation 2).

It should be noted that using the expanded system does not completely solve the stability problem; below the shear turnover depth the system is still inherently unstable. Further, the maximum exponent size available on a computer will impose a practical limit on the maximum frequency of any reflectivity computation. However, whenever instability or overflow problems occur in a reflectivity computation it is usually legitimate to redefine the structure to

eliminate the problem (Fryer, 1978). No such problems were encountered in any of the analyses reported here. An improvement on the expanded system which completely solves the stability problem has been discovered by Abo-Zena (1979), but as stability was not a bad problem in this study the Abo-Zena modification was not used. The reflectivity computations reported here were performed only for real angles of incidence at the ocean bottom. If the study had been extended to apparent velocities lower than the sound speed in water to include the inhomogeneous waves that result from complex angles of incidence as described by Frisk (1979) and Stephen (1977), stability would have been a problem and the Abo-Zena modification would have been necessary.

All the analyses reported here were performed using the fifth-order system, but for conciseness only the fourth-order system will be described in the remainder of this paper.

C. Perturbing the Solution

Equation (3) (or strictly, equation 17) can be solved directly by numerical integration. However, the form of the homogeneous layer solution is simple, so it seems more reasonable to treat the effects of varying elastic parameters as a perturbation on that solution. This is the approach favored by Takeuchi and Saito (1972). Rather than accept the approximate equality between the true subinterval propagator and the homogeneous layer propagator (equation 14), we can

write

$$P(z, z_k) = D(z, z_k) \Delta P(z, z_k) \quad (18)$$

where ΔP is the perturbing effect of variable elastic properties.

Since $P(z, z_k)$ and $D(z, z_k)$ become the identity at $z = z_k$, then

$$\Delta P(z_k, z_k) = I.$$

In fact ΔP is the matricant of the system

$$\frac{d}{dz} \Delta P(z, z_k) = \Delta A(z) \Delta P(z, z_k), \quad (19)$$

where

$$\Delta A(z) = D^{-1}(z, z_k) C(z) D(z, z_k) \quad (20)$$

(Pease, 1965, p. 176-177). This means that instead of solving equations (3) we can choose to solve (19) and construct the subinterval propagator using equation (18).

Numerical solution of equation (19) requires repeated evaluation of the system matrix ΔA . This appears to be an expensive operation as ΔA involves the complex matrix inverse D^{-1} . However, it can be readily be verified that D^{-1} has elements

$$(D^{-1})_{ij} = (-1)^{i+j} (D)_{ij},$$

so no actual inversion need be performed. The matrix D also has the property that it is symmetrical about the trailing diagonal, which results in ΔA having the highly symmetric form

$$\Delta A = \begin{pmatrix} \Delta a_{11} & \Delta a_{12} & \Delta a_{13} & \Delta a_{14} \\ \Delta a_{21} & \Delta a_{22} & \Delta a_{23} & -\Delta a_{13} \\ \Delta a_{31} & \Delta a_{32} & -\Delta a_{22} & \Delta a_{12} \\ \Delta a_{41} & -\Delta a_{31} & \Delta a_{21} & -\Delta a_{11} \end{pmatrix}$$

so ΔA can be rapidly evaluated.

Because $C(\zeta_k) = A(\zeta_k) - A_k = 0$, the system (19) is well suited to solution by a fourth-order Runge-Kutta procedure. The Runge-Kutta solution of equation (19) is

$$\Delta P(z_{k+1}, z_k) = I + \frac{\Delta z_k}{6} [\Delta A(z_{k+1}) + \Delta A(z_k)]$$

so that the desired subinterval propagator is, from equations (18) and (20),

$$P(z_{k+1}, z_k) = D_k + \frac{\Delta z_k}{6} [D_k C(z_k) + C(z_{k+1}) D_k] \quad (21)$$

(Takeuchi and Saito, 1972). Here the propagator P is expressed as the sum of the homogeneous layer term and a term resulting from variation of elastic parameters with depth. If the subinterval is truly

homogeneous then $C(z)$ is identically zero and the second term becomes zero, as expected. The Runge-Kutta procedure can be very efficiently coded so that computation of P from equation (21) takes only twice as long as the Thomson-Haskell result D .

D. A Comparison of Codes

A typical comparison of the Thomson-Haskell and Runge-Kutta solutions is shown in Figure 2. The two methods were used to compute the reflectivity for the structure of Table I; this structure is not meant to represent any sensible sedimentary sequence but was chosen to accentuate the differences between the two methods. Fig. 2 shows reflectivities for an angle of incidence of 60° , plotted as a function of frequency. Thomson-Haskell estimates are plotted on the left and Runge-Kutta on the right. Each reflectivity plot shows the modulus of the calculated reflectivity and of the "theoretical" reflectivity computed using the Thomson-Haskell method with the gradient zone approximated by 100 homogeneous layers. The "error" plots show the absolute difference between the computed and "theoretical" reflectivities. Runge-Kutta results for n steps are displayed next to $2n$ step Thomson-Haskell results as these are directly comparable in terms of computation time.

It is immediately apparent from Fig. 2 that both methods converge satisfactorily towards the true solution. In general, for the same computation time, the Runge-Kutta approach is more accurate at low

Figure 2. Comparison of Thomson-Haskell (TH_n) and Runge-Kutta (RK_n) reflectivity estimates for the test structure of Table I. The angle of incidence is 60°. Each estimate is plotted with the "theoretical" reflectivity of a 100-step Thomson-Haskell integration (bold line). The absolute difference between each estimate and the "theoretical" is plotted as "error." A 2n-step TH estimate requires identical computation time to an n-step RK.

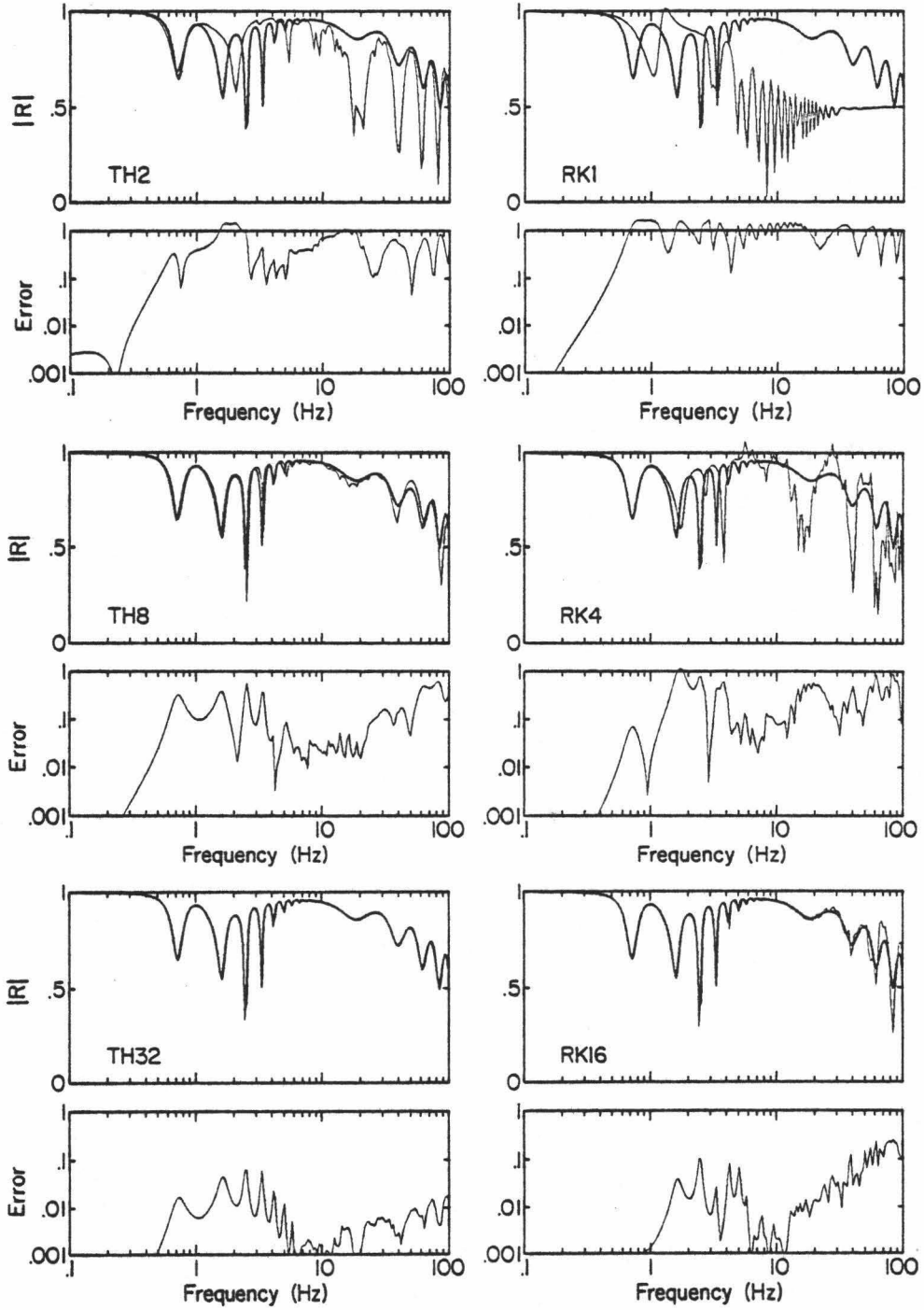


TABLE I
 Test Structure with High Gradients*

Depth m	α m/s	β m/s	ρ g/cm ³	Q_α	Q_β
Water	1520	---	1.00	---	---
0	1500	100	1.50	250	25
300	2250	1300	1.80	250	25
Basement	8000	4700	3.4	1000	460

* Velocity and density increase linearly from 0 to 300m.

frequencies, the Thomson-Haskell at high frequencies, with the superiority of the Runge-Kutta method extending to higher and higher frequencies as the step size is reduced. A more detailed analysis shows that the Runge-Kutta approach always converges more rapidly than the Thomson-Haskell. This behaviour is not unexpected. The Thomson-Haskell method is essentially a second order integration scheme, the Runge-Kutta method used here is fourth order; in general, higher order methods converge more rapidly. The superior accuracy of the Thomson-Haskell method at low levels of approximation is because the method yields exact results for an approximate Earth model. This means Thomson-Haskell reflectivities always make physical sense and the occasional erratic results of the Runge-Kutta method (such as reflectivities greater than unity) are avoided.

No matter for what purpose theoretical reflectivities are calculated, to apply them to any problem in the real world involves the double transformation necessary to travel between ω - k and time-distance space. These transformations are either performed numerically or by using some analytic approximation, but in either case noise is introduced. This means that even if the physical nature of the structure under investigation were known to great accuracy (which is never the case), computing reflectivities to within an absolute error of about .005 would be unjustified. Since only modest accuracy is necessary, the Thomson-Haskell method must be the preferred approach, in keeping with the finding that for low accuracy problems in general low order methods are the most practical (Gear, 1971, p. 73-76).

E. Adaptive methods

The Thomson-Haskell and Runge-Kutta methods described above were used in a crude manner with the integration performed by marching along with a preselected step size in ignorance of the error behaviour. There are, however, numerous adaptive procedures available which automatically modify their step size to keep errors below specified limits. A number of these were investigated both by solving the original propagator equation (equation 3) and by solving for the perturbation (equation 19). The codes used were the adaptive Runge-Kutta code RKF45 of Watts and Shampine (Forsythe, et al, 1977, p. 129-147), two codes based on Adams' method: DE/STEP by Shampine and Gordon (1975) and DIFSUB by Gear (1971, p. 155-167), and the rational extrapolation code of Gear (1971, p. 93-101). These codes are generally regarded as the most efficient general-purpose codes available (Shampine, et al, 1976). On some occasions DE/STEP detected stiffness, so DIFSUB was also used in its stiff configuration.

All the adaptive procedures considered were successfully used to compute reflectivities, and performed the useful task of verifying the Thomson-Haskell results. The fastest adaptive procedure was to use RKF45 in solving equation (3), although this was only marginally faster than the other methods. The adaptive methods easily outperformed the Thomson-Haskell for high accuracy results, but took between five and ten times longer for more justifiable accuracies. When computing a suite of reflectivities at 50 different frequencies, the adaptive methods were often two orders of magnitude slower than

the Thomson-Haskell. This poor performance is partially a consequence of low order methods being superior for low accuracy problems, but the major reason is more profound. An adaptive procedure could probably be modified to compute a single reflectivity estimate as rapidly as the Thomson-Haskell method, but a single reflectivity estimate contains little useful information. Because of the need to perform a double transformation, what is required is that the reflectivity surface be defined over a finite range in ω - k space. This implies repetitive computation of the reflectivity for a range of frequencies and wavenumbers. The Thomson-Haskell method can be used with the same step size for all points in ω - k space so that many intermediate computations need be performed only once. By comparison, each reflectivity computation by an adaptive method is essentially independent, so there is little advantage in keeping intermediate results. The adaptive methods could certainly be recoded for more efficient computation of reflectivities, but it is unlikely that any adaptive code could be made as practical as the Thomson-Haskell method.

IV. GRADIENT-DRIVEN P-SV COUPLING

Having accepted that the Thomson-Haskell method provides the most efficient means of computing reflectivities, we can apply the method to an assessment of the importance of coupling between compressional and shear disturbances. In this section we consider the structure of Fig. 1, a sedimentary sequence between two halfspaces. We assume there are no first-order discontinuities within the sediments and approximate the sequence by $n-1$ thin homogeneous layers.

To evaluate the importance of P-SV coupling caused by gradients it is necessary to solve not for the stress propagator P but the potential propagator E which contains the explicit coupling terms. The relationship between the wave potentials $\Phi_1(z_1)$ and $\Phi_{n-1}(z_n)$ at the top and bottom of the sediments is

$$\Phi_{n-1}(z_n) = E(z_n, z_1)\Phi_1(z_1).$$

The potential vector ϕ has the general form of equation (8), so if there is no coupling between P and S arising from gradients, E will have the form .

$$E(z_n, z_1) = \begin{pmatrix} e_{11} & 0 & e_{13} & 0 \\ 0 & e_{22} & 0 & e_{24} \\ e_{31} & 0 & e_{33} & 0 \\ 0 & e_{42} & 0 & e_{44} \end{pmatrix} \quad (22)$$

This is the form assumed by Vidmar and Foreman (1979), who wished

explicitly to leave P-S coupling out of their analysis. If coupling does exist, then E will, in general, have no zero terms. This suggests a simple procedure for assessing the importance of coupling: Reflectivities can be computed twice, first by assuming that E has the form of equation (22), and second, by considering the complete response. Any difference between the two sets of results must be a consequence of coupling.

From equation (5) the stress and potential propagators are related by

$$P(z_n, z_1) = T_n^{-1} E(z_n, z_1) T_1$$

so from equations (15) and (16) it is apparent that

$$E(z_n, z_1) \approx \exp(\Lambda_{n-1} \Delta z_{n-1}) D_{n-1} D_{n-2} \dots D_3 D_2 \exp(\Lambda_1 \Delta z_1)$$

hence E may readily be computed. The most efficient computation method would be to use a scheme based on potentials rather than stress and displacement, such as the phase-related coefficient method of Kennett (1974). However, the traditional Thomson-Haskell procedure of computing Haskell layer matrices D may readily be modified to isolate the potential propagator. That was the method used here.

V. RESULTS

A. Model 1

The initial subject chosen for P-S coupling investigations was the structure analysed by Fryer (1978) and Vidmar and Foreman (1979), shown in Figure 3. We shall refer to this structure as Model 1; details of the structure are given in Table II. Model 1 is consistent with data on silt clays, turbidites and mudstones compiled by Hamilton (1976a,b, 1978, 1979b) and is assumed to be representative of the higher velocity and density gradients to be found in a marine sedimentary sequence. The structure has continuously varying elastic properties with linear variation of all parameters from 0 to 36m, 36 to 120m, and 120 to 650m below the ocean bottom. Each of these three sections was approximated by a series of homogeneous layers, the number of layers being determined by convergence tests such as that illustrated in Fig. 2. Somewhat stricter convergence criteria were imposed than in the original study (Fryer, 1978) so more layers were used in the approximation. In Table II attenuation is defined by the quality factor Q . The reciprocal, Q^{-1} , was assumed to vary linearly with depth. For convenience the equivalent attenuation coefficients have been included in the table.

Figure 4 shows the modulus of the total reflectivity function for Model 1 for frequencies from 0.1 to 10 Hz and angles of incidence from normal to grazing. The surface has frequency-independent ridges at 20° and 40° marking critical incidence at basement of P waves and S

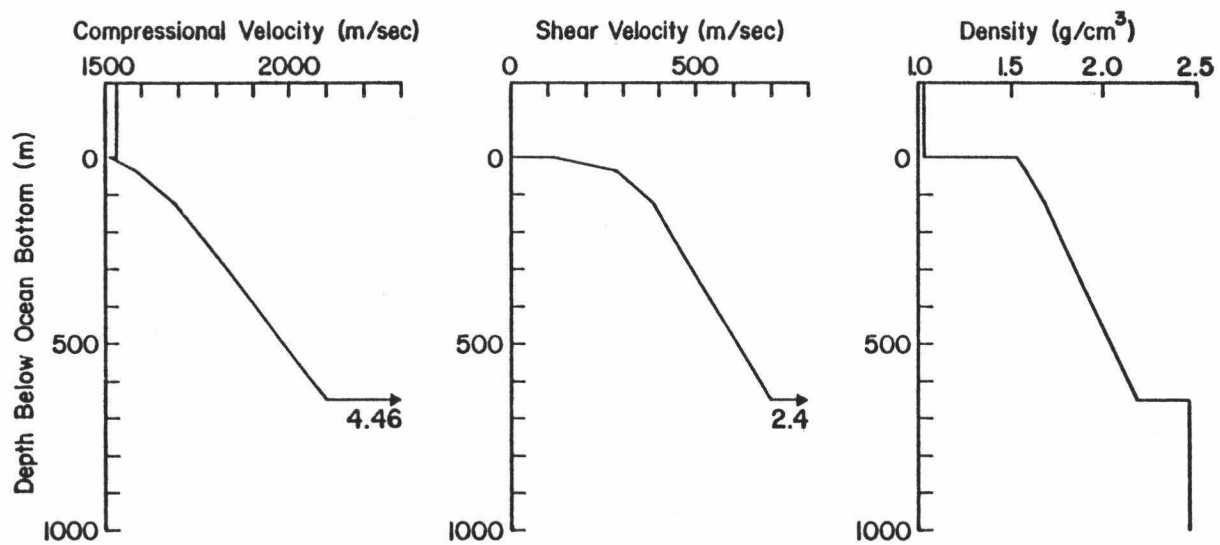


Figure 3. Parameters of Model 1. See Table II for details.

TABLE II

Model Parameters

Depth m	α m/s	β m/s	ρ gm/cm ³	Q_α	Q_β	k_α dB/m-kHz	k_β dB/m-kHz	No. of layers from previous depth
<u>Model 1</u>								
Water	1530	--	1.03	∞	--	0	--	
0	1510	116	1.53	278	27.8	.065	8.46	
36	1582	283	1.58	172	17.2	.100	5.61	6
120	1675	391	1.69	100	10.0	.163	6.98	8
650	2100	699	2.18	120	12.0	.108	3.25	8
Basement	4460	2400	2.46	750	290	.008	.0039	
<u>Model 2</u>								
Water	1530	--	1.03	∞	--	0	--	
0	1510	10	1.45	3000	30	.0060	90.9	
4	1518	74	1.47	2780	33	.0065	11.2	5
36	1582	283	1.58	2500	160	.0069	0.603	15
120	1685	391	1.69	1475	160	.011	0.436	8
650	2100	699	2.18	1200	209	.011	0.187	8
Basement	4460	2400	2.46	750	290	.008	0.039	

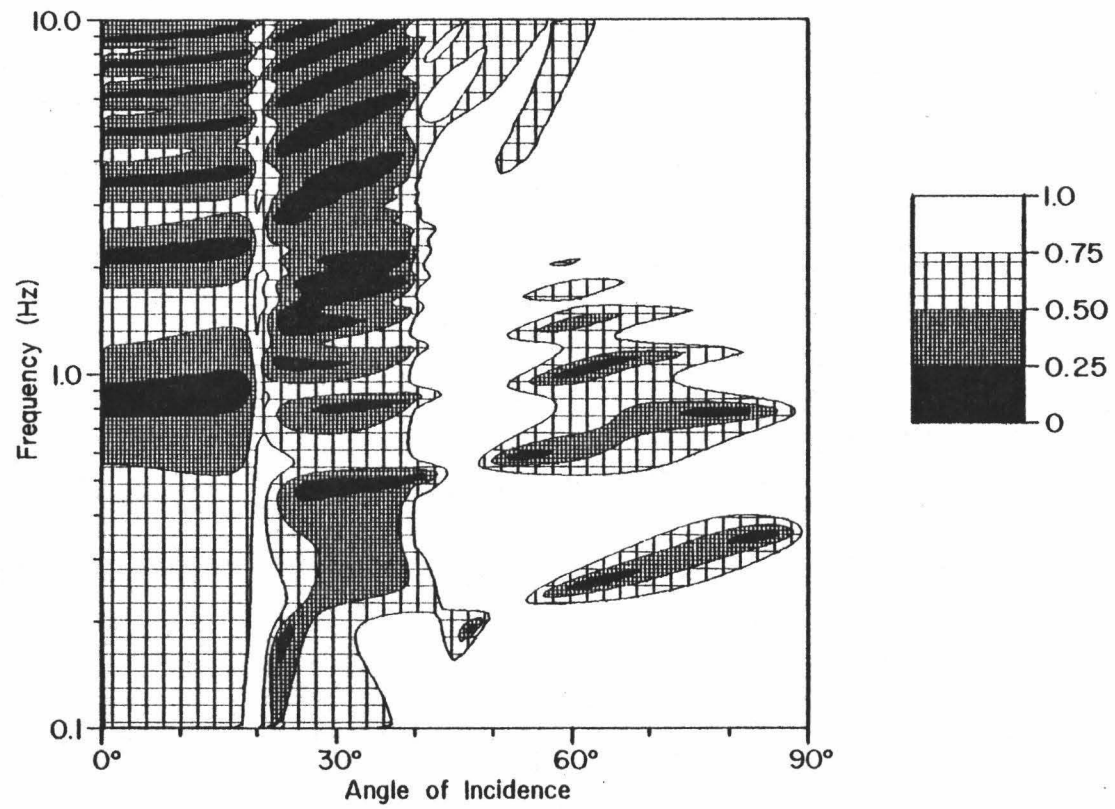


Figure 4. Modulus of the reflectivity function for Model 1.

waves respectively. From normal incidence to the P critical angle the reflectivity surface is dominated by resonance of compressional waves reflected between the sediment-water and sediment-basement interfaces. From the shear critical angle to grazing incidence, a similar shear resonance explains the low-frequency structure (below 3 Hz); at higher frequencies the absorption is caused by P waves reaching turnover depth within the sediment column. This P structure is much better developed above 10 Hz (Fryer, 1978). Between the two critical angles the reflectivity is a complicated function presumably caused by P and S resonances and interconversions.

To determine the explicit effects of shear propagation on the reflectivity the function was recomputed assuming fluid sediments (i.e. sediments with vanishingly small shear velocity). The results are shown in Figure 5. It is apparent that for angles of incidence greater than the shear critical angle (40°), the shear effects are only important below 3 Hz. However, shear effects are strongly dependent on the shear attenuation structure; if the shear attenuation were appreciably less than has been assumed here, shear conversions would be important to higher frequencies. Comparing Fig. 5 with the similar plots of Mitchell and Lemmon (1979), it is apparent that in the absence of shear conversions, the reflectivity can very simply be computed using their ray theory approach.

Shear conversion can occur at interfaces and as a consequence of gradients; the above analysis cannot differentiate between the two. To determine the importance of gradient-driven P-S coupling, the reflectivity function of Fig. 4 was recomputed with the P-S coupling

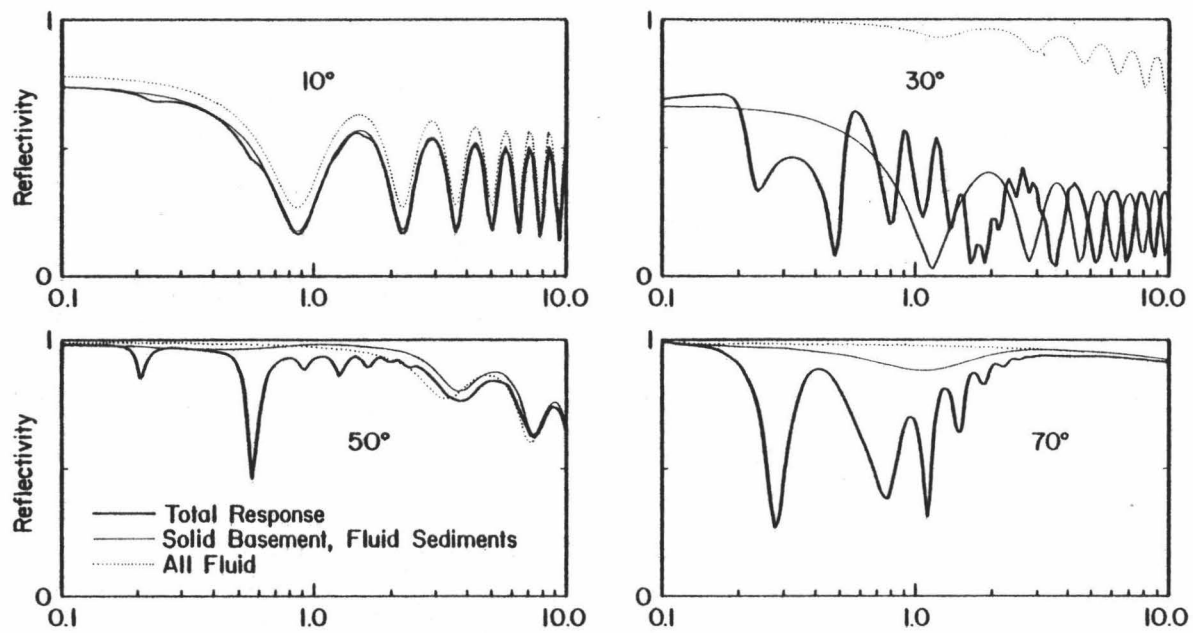


Figure 5. The effects on reflectivity of ignoring shear propagation for various angles of incidence. The structure is Model 1.

terms of the potential propagator set to zero as described in section IV. The difference in magnitude between the total reflectivity and the partial reflectivity (with the gradient-driven coupling ignored) is shown in Figure 6 and the difference in phase in Figure 7. The coupling function is complicated but is fairly simply interpreted once the different features are recognised. Coupling seems to affect the energy transmitted through the zone of high gradients much more than the backscattered energy. For the transmitted energy to affect the bottom reflectivity it must reappear at the surface. For angles less than 20° little of the transmitted energy is reflected from basement and most escapes into the lower halfspace. Beyond 20° compressional energy is supercritically reflected from basement so the coupling effects are seen. Between 20 and 40° coupling affects the compressional energy reflected from basement. The phase errors (Fig. 7) are mostly positive over this range which means that more energy is propagating as compressional waves than would be the case if coupling were absent. This interpretation is justified later through a consideration of time functions. Beyond 40° incidence, shear energy too is supercritically reflected from basement. The features seen in Figs. 6 and 7 are thus a combination of the two patterns arising from supercritical reflection of the two types of waves, one pattern starting at 20° , the other at 40° . The null that appears at 48° in the plot of phase errors (Fig. 7) is just a consequence of the interference between the two patterns. It is purely fortuitous that the minimum angle for compressional wave refractions within the sediments is also at 48° ; P turnover within the sediments does not

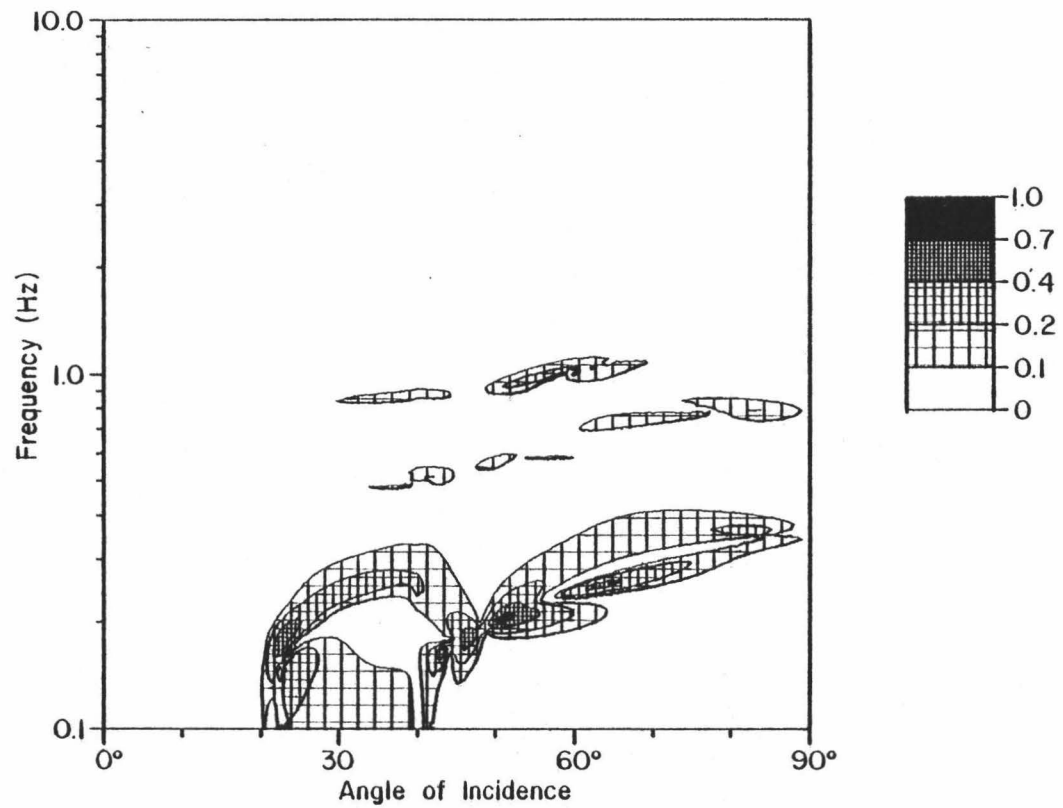


Figure 6. Error in the magnitude of the reflectivity function for Model 1 if decoupling is assumed.

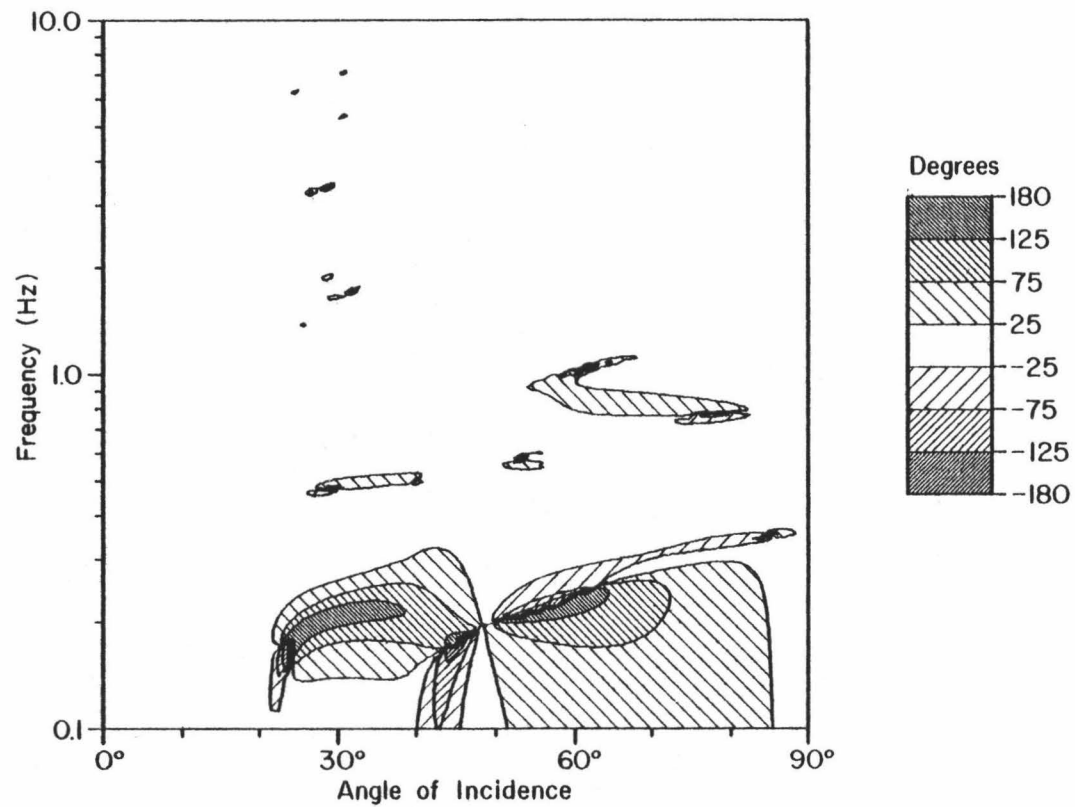


Figure 7. Error in the phase of the reflectivity function for Model 1 if decoupling is assumed.

affect the coupling as will be shown later when the effects of sediment thickness are considered. It might be argued that P-wave turnover in the sediments would induce Stoneley waves on the sediment-basement interface (Hawker, 1978). If this occurs it certainly does not affect gradient-induced P-S coupling. The coupling peaks seen here occur at a about 0.2 Hz so the interface wave would have such a long wavelength that it would also sense the water-sediment interface. Under such conditions a Stoneley wave travelling faster than the speed of sound in water could not be sustained. Again, consideration of the sediment thickness will show that Stoneley wave propagation is unimportant to coupling for real angles of incidence.

The effects of coupling become dramatic below 0.5 Hz, this is probably too low a frequency for the effect to be of much importance in most problems. This becomes more apparent when a detailed comparison of the total and partial reflectivities is made. Such a comparison is shown for a range of angles of incidence in Figures 8 to 11. Each of these figures shows both reflectivities and the absolute difference between them, labelled "error." The inverse Fourier transform of the reflectivity, a time series termed the plane-wave response, is also plotted; this is a function of intercept time at the ocean bottom (Fryer, 1980, reproduced here as Appendix B). (If a wave travelling at an apparent velocity c takes a time t to get from the ocean bottom to turnover depth and back and if it emerges at the ocean bottom a distance x from its point of incidence, then the intercept time at the ocean bottom is $t-x/c$). Near normal incidence coupling is

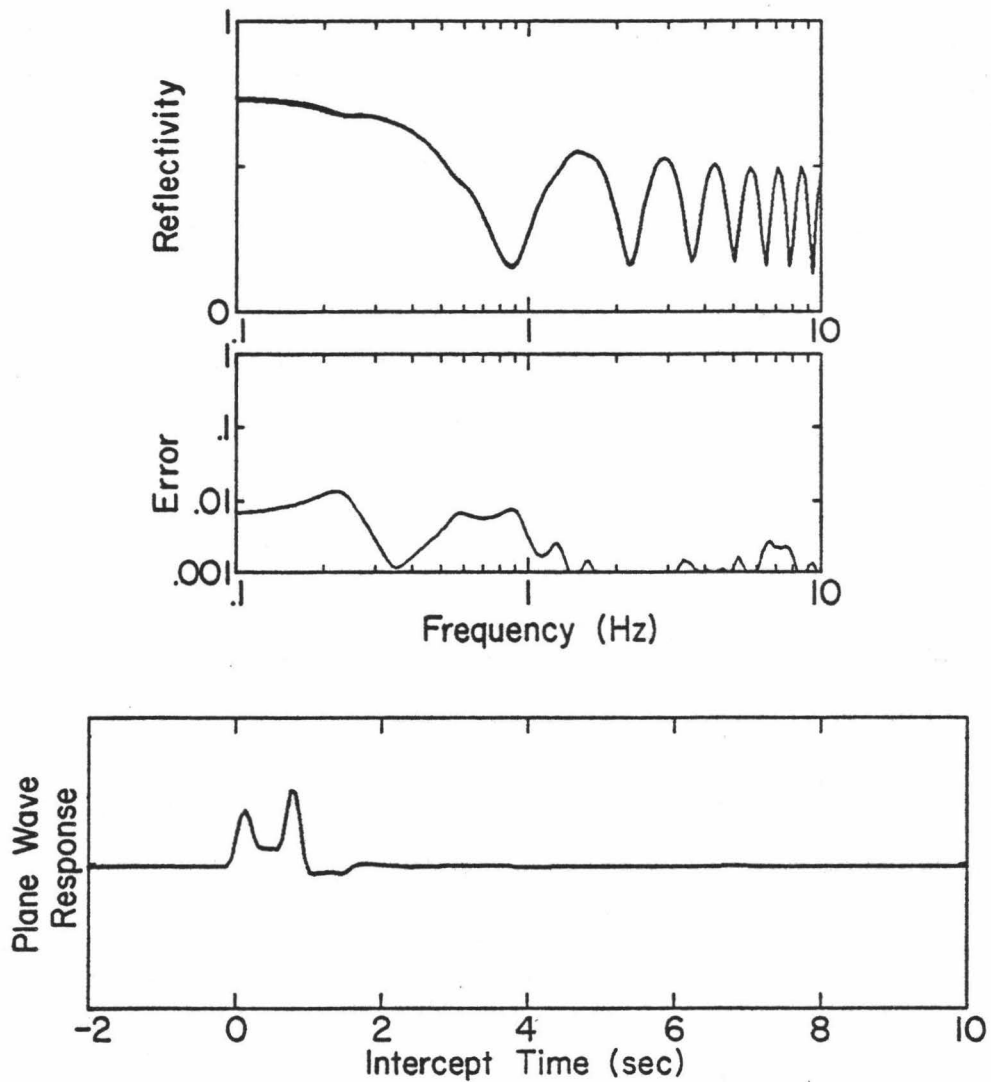


Figure 8. Comparison of total and partial (decoupled) reflectivities for Model 1 at an angle of incidence of 10° . The error curve is the absolute value of the difference. The plane-wave response (the inverse Fourier transform of the reflectivity) is also shown.

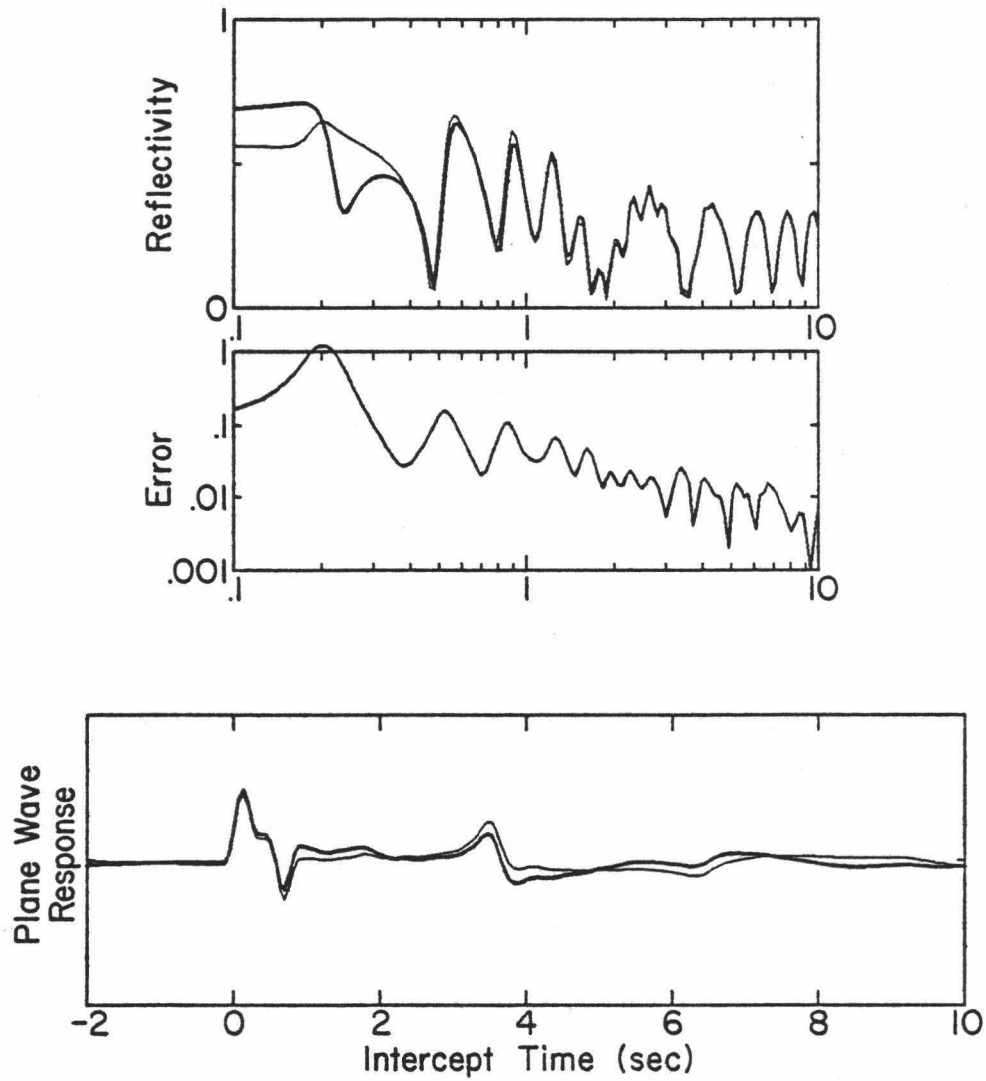


Figure 9. As Figure 8 but for an angle of incidence of 30° . On both the reflectivity and plane-wave response plots the bolder curve is the total solution.

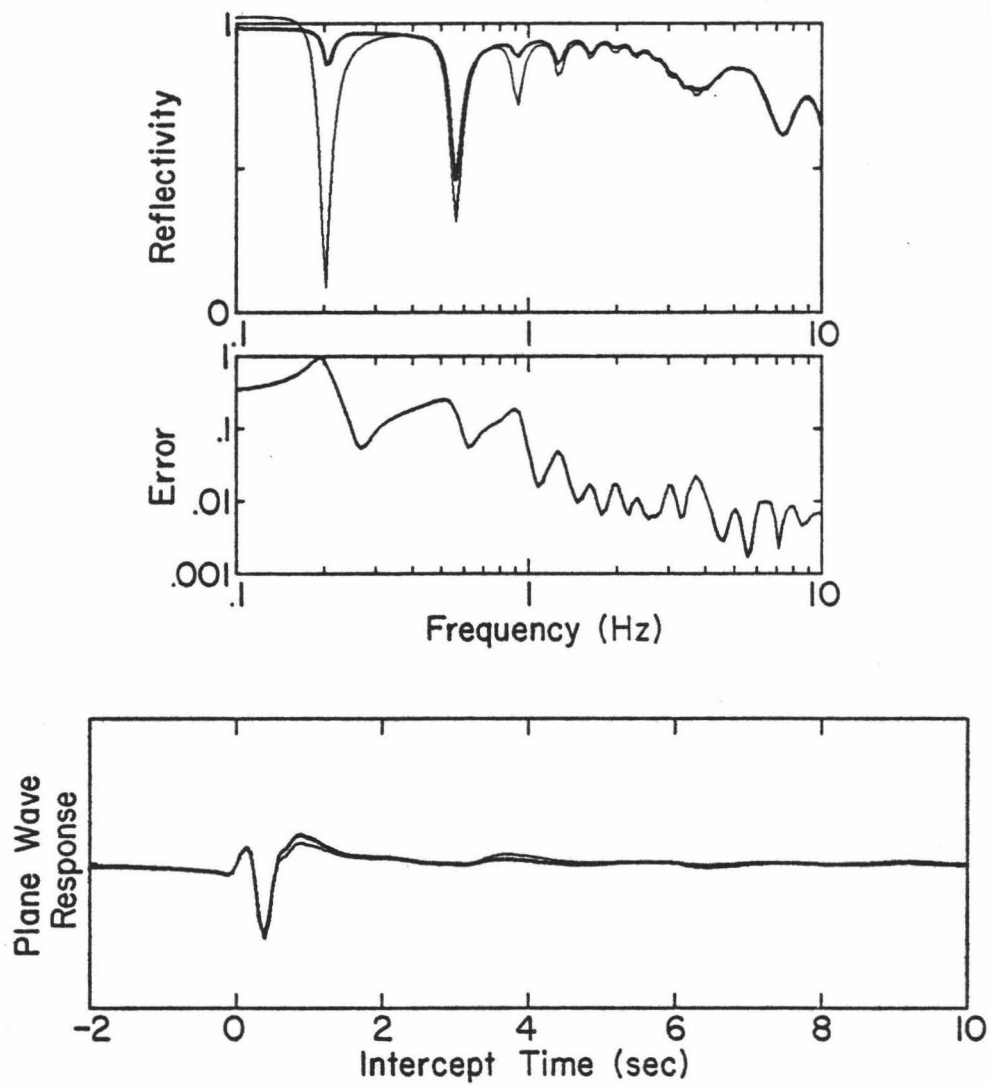


Figure 10. As Figure 9 but for an angle of incidence of 50° .

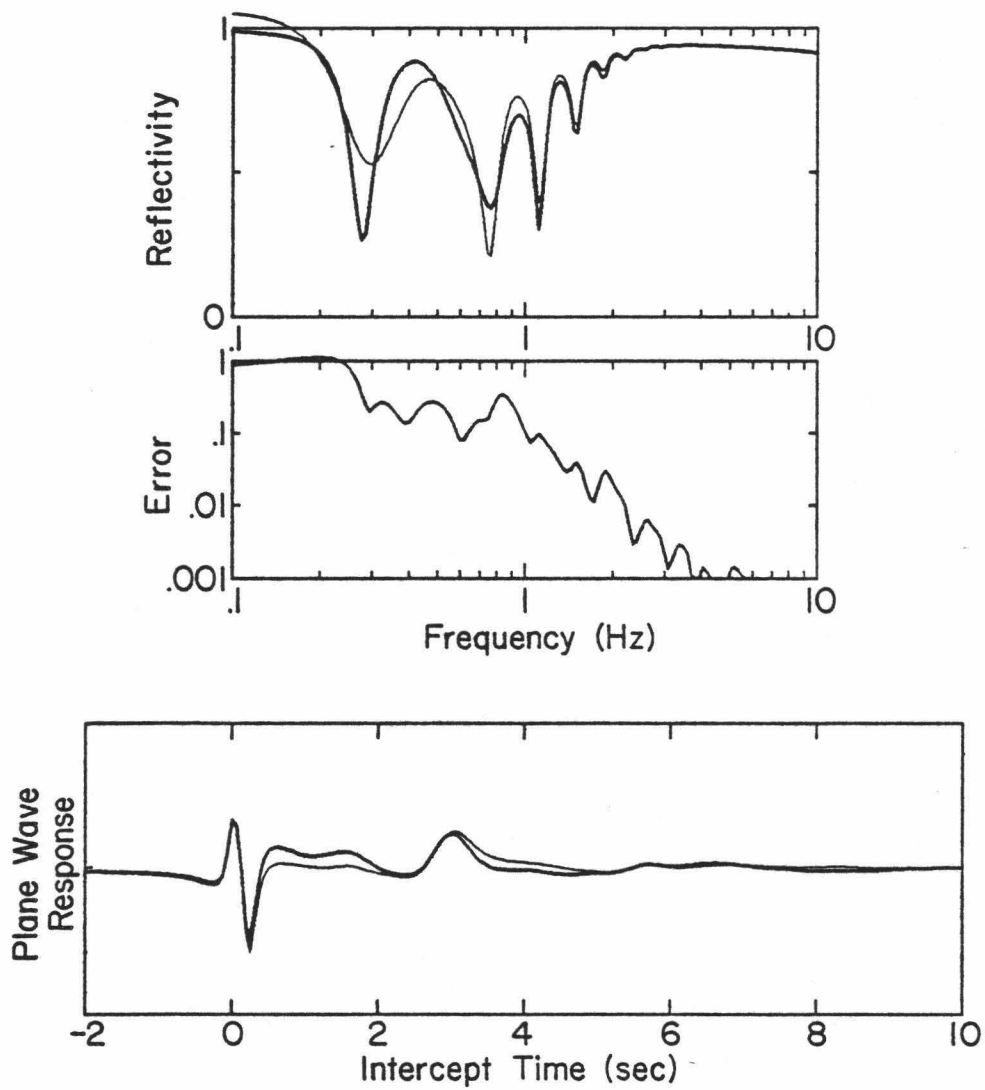


Figure 11. As Figure 9 but for an angle of incidence of 70° .

expected to be small, this is verified by Fig. 8 for an angle of incidence of 10° . The error in the partial reflectivity is everywhere small and the only discernable coupling occurs below 0.2 Hz. The plane wave response shows a doublet of arrivals; these are the bottom and basement reflections. Some energy in the bottom reflection spills forward before the theoretical intercept time of zero, in part because of zero-phase-shift filtering and in part because of the manner in which attenuation has been included in the model. We have assumed that Q is independent of frequency (i.e., that attenuation is proportional to frequency). This assumption violates causality (Strick, 1967), but the effect is not troublesome if a wide frequency band is used in the analysis.

At 30° (Figure 9) the gradient-driven coupling is important, but only below 0.4 Hz. The error at 0.2 Hz exceeds unity because the phase error is close to 180° (see Fig. 7). At 30° compressional energy is supercritical at basement so in the plane-wave response the basement reflection appears as a negative pulse. The strong emergent arrival with an intercept time of about 3 seconds is the PSSP phase, this is energy which has converted to shear at the water-sediment interface and reflected off basement, making two passages through the sediments as a shear wave. Its multiple appears at 6 seconds intercept time. The effect of gradient-driven coupling at this angle is to add energy to the tail end of the P-reflection group of arrivals at the expense of the PSSP phase. A possible explanation is that part of the shear energy resulting from P-S conversion at the sediment-water interface is converted back to P in the zone of high

velocity gradient at the top of the sediments. Because this energy has travelled part of the way as a shear wave it is delayed relative to the normal P group, explaining the drawn-out tails of the P arrivals. This energy is denied to the PSSP phase, which is weaker as a result.

At 50° (Figure 10) coupling effects can be seen in the reflectivity up to 4 Hz, but above 1 Hz the effects are very minor. Ignoring the coupling leads to a slight mismatch of stresses at the sediment-water interface (i.e. a violation of boundary conditions) which explains the reflectivity greater than unity at 0.1 Hz. The bottom reflection appears as a positive pulse in the plane-wave response, as it must for all angles of incidence because of the P-velocity inversion at the top of the sediments. The negative pulse is now the P refraction in the sediments rather than a basement reflection as P energy reaches turnover above basement at a depth of 524m in the sediments. The theoretical intercept time for this arrival is 0.26 sec. Again the effect of coupling is to extend the P group of arrivals and reduce the energy of the PSSP phase, but the effect is very small.

The description above for 50° holds also for 70° (Figure 11). The chief difference is that the error in the partial reflectivity now falls more rapidly with frequency. Again, coupling effects are only important below 1 Hz. The bottom reflection and sediment refraction are now only 0.02 sec. apart in intercept time (too close to resolve here). As at the other angles of incidence, coupling extends the P arrivals at the expense of the PSSP. It is apparent that at all

angles of incidence gradient-driven P-S coupling only affects the response of the bottom at frequencies below 1 Hz and that its effect is probably never appreciable enough to be of any concern in long-range propagation problems.

Although the plane-wave response is a time function it is not directly observable in practice because it is impossible to isolate the effects of a discrete angle of incidence (ignorance of this fact leads to inconsistencies such as negative bottom loss). The observable response can be synthesized by performing the Hankel transformation necessary to convert a function of angle of incidence (or wavenumber) to distance. That was done here following the reflectivity-slowness method of Fryer (1980; Appendix B). The results are shown in Fig. 12, a record section plotted on a reduced time scale with a reduction velocity of 2 km/sec. The figure shows the smoothed response of the ocean bottom to a pressure pulse at the surface of a 5 km deep isovelocity ocean, as observed at the ocean surface. Results using both the total and partial responses are shown. The direct ray between source and receiver and surface-reflected phases have been ignored. A ray interpretation of the arrivals of Figure 12 is shown in Figure 13. At long range the bottom reflection is part of a complex of arrivals lasting half a second and including the P refractions within the sediments. In the frequency band investigated here (0 to 10 Hz) it is not possible to resolve these arrivals. At short range the two positive pulses are the bottom and basement reflections; the later basement reflection being a little stronger. At 10 km and greater ranges the headwave from basement is the first

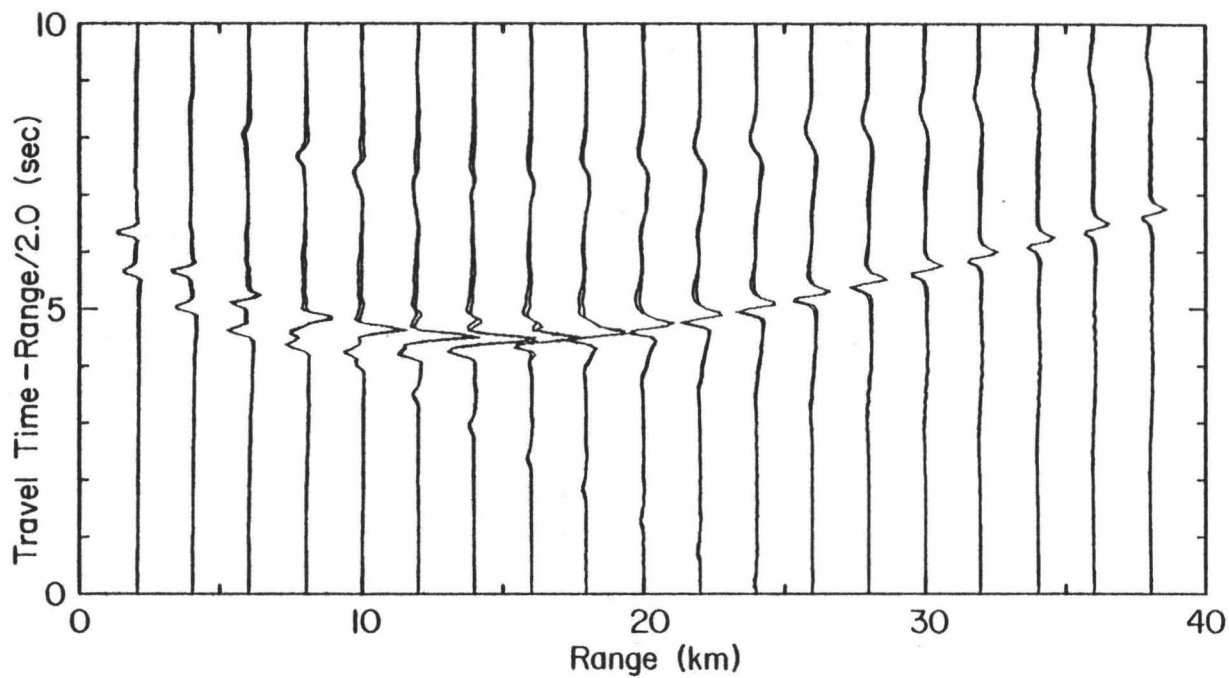


Figure 12. Synthetic pressure records for Model 1 computed from total and partial reflectivities. The ocean is assumed to be 5km deep and source and receiver are at the surface. The direct and surface-reflected phases have been ignored. Traces are amplified proportional to the square root of the range.

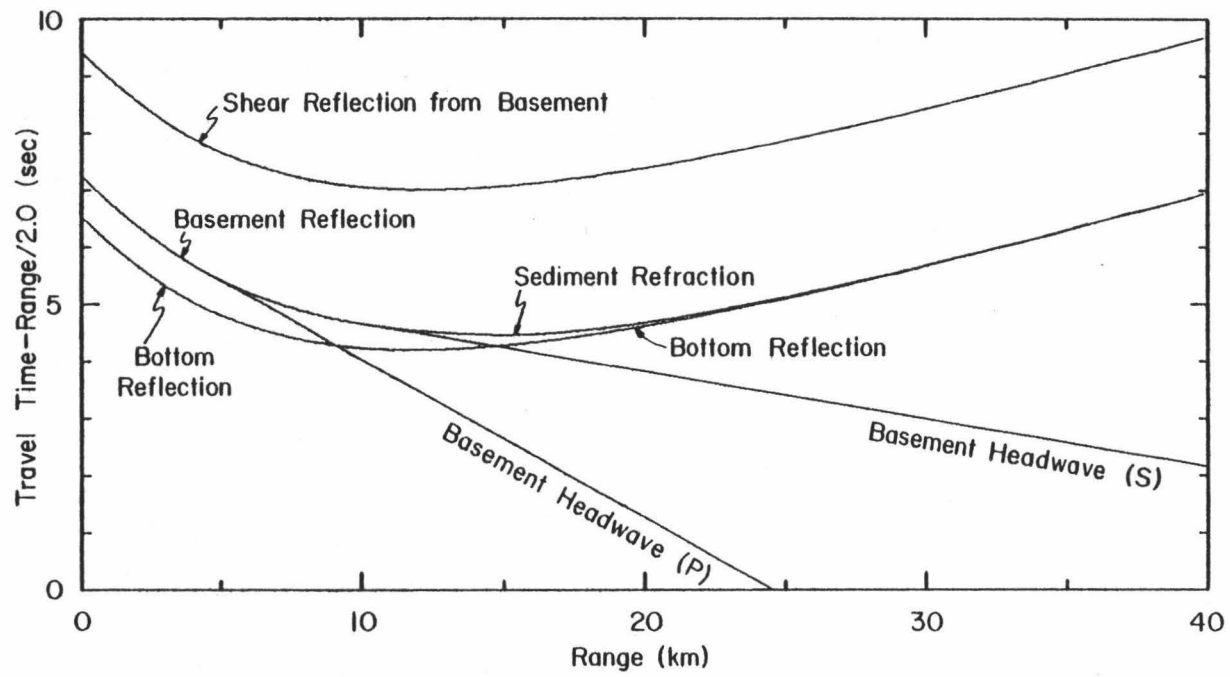


Figure 13. A ray interpretation of Figure 12.

arrival. As expected this is a very weak phase which decays rapidly with distance. The weak arrival appearing at all but the closest ranges three seconds after the main reflection branch is the PSSP phase. The minor noise beyond 25 km is introduced by the crude integration scheme used to evaluate the Hankel transform.

Comparing the total and partial responses shown in Fig. 12 it appears that gradient-driven coupling only has discernable effect between 5 and 25 km range. As expected from the behaviour of the plane-wave response (Figs. 8-11) the effect of this coupling is to increase the energy in the tail of the P group of arrivals and reduce the subsequent PSSP energy. However the effect is extremely small. Because of the increase in ambient noise at low frequencies, it is unlikely that ignorance of these coupling effects would lead to important errors in the prediction of long-range propagation loss. Indeed, it would be extremely difficult to measure the coupling experimentally except, perhaps, in studies of Stoneley waves on the sediment-water interface. It is probable that the only practical means of studying the effects of coupling on body waves would be to use natural sources (earthquakes) which are rich in low frequency energy.

B. Model 2

It must be emphasised that the claim that gradient-driven coupling can be ignored is only as valid as the model. If velocity gradients in an actual ocean bottom are ever much above those of Model 1 the gradient-driven coupling might become important. The variation of compressional wave velocity with depth is fairly well known, with velocity gradients seldom exceeding the value of 2.0/sec used in Model 1 (Hamilton, 1979a). However shear velocities and shear velocity gradients are very poorly known and may well be poorly represented by the model values. Presumably in a quiet environment where the ocean bottom is essentially a sediment suspension the initial shear velocity may start out at zero and increase extremely rapidly with depth. In work on Stoneley waves Davis (1965) estimated an initial shear velocity gradient of 16/sec, considerably greater than the 4.65/sec of Model 1. Although the very low shear velocity and high gradient apply only to the first few meters this still might affect low-frequency propagation as very low wave speeds mean that even low-frequency waves will have fairly short wavelength. To investigate the consequences of low shear velocities and high gradients, Model 2 of Table II was analysed. This model is not meant to represent any real ocean bottom but was chosen to have the maximum shear velocity gradient and minimum attenuations possible and still be consistent with observed data. The compressional velocity structure of Model 2 is identical to Model 1 and the density structure only marginally different with a slightly lower surface density. The surficial sediments have a shear velocity

of 10m/sec, considerably less than any reported in situ velocity, but higher than the minimum laboratory measurement of Shirley and Hampton (1978). The initial shear velocity gradient is 16/sec, consistent with Davis' result. The attenuation structure of Model 2 is considerably different from Model 1. There is considerable evidence that compressional wave attenuation has been overestimated in the past (Helmberger et al., 1979; Mitchell and Focke, 1980), and this may be the case for shear waves also. The compressional-wave Q structure of Model 2 essentially follows the results of Mitchell and Focke (1980). For shear waves, the attenuation by surficial sediments was chosen to be the minimum of the range of values presented by Hamilton (1976b), a logarithmic decrement of 0.1. Q^{-1} was assumed to decrease linearly with depth to a depth of 36m where shear and compressional attenuations are related by $Q_{\alpha}/Q_{\beta} = 0.5\alpha^2/\beta^2$. This relationship was assumed to hold for the rest of the sediments.

The modulus of the reflectivity function for Model 2 is shown in Figure 14. For angles of incidence of less than 20° this is identical to the function for Model 1 (Fig. 4) since the compressional velocity structures are the same. The greatest difference in the reflectivity between the two models occurs at large angles of incidence. The shear absorption fringes are much closer spaced in frequency for Model 2 than Model 1, presumably because the mean shear velocity in the sediments is considerably less. The fringes decay less rapidly with frequency because of the lower attenuation. If gradient-driven coupling is ignored in Model 2 the magnitude and phase error of the resulting reflectivity are as shown in Figures 15 and 16. These are

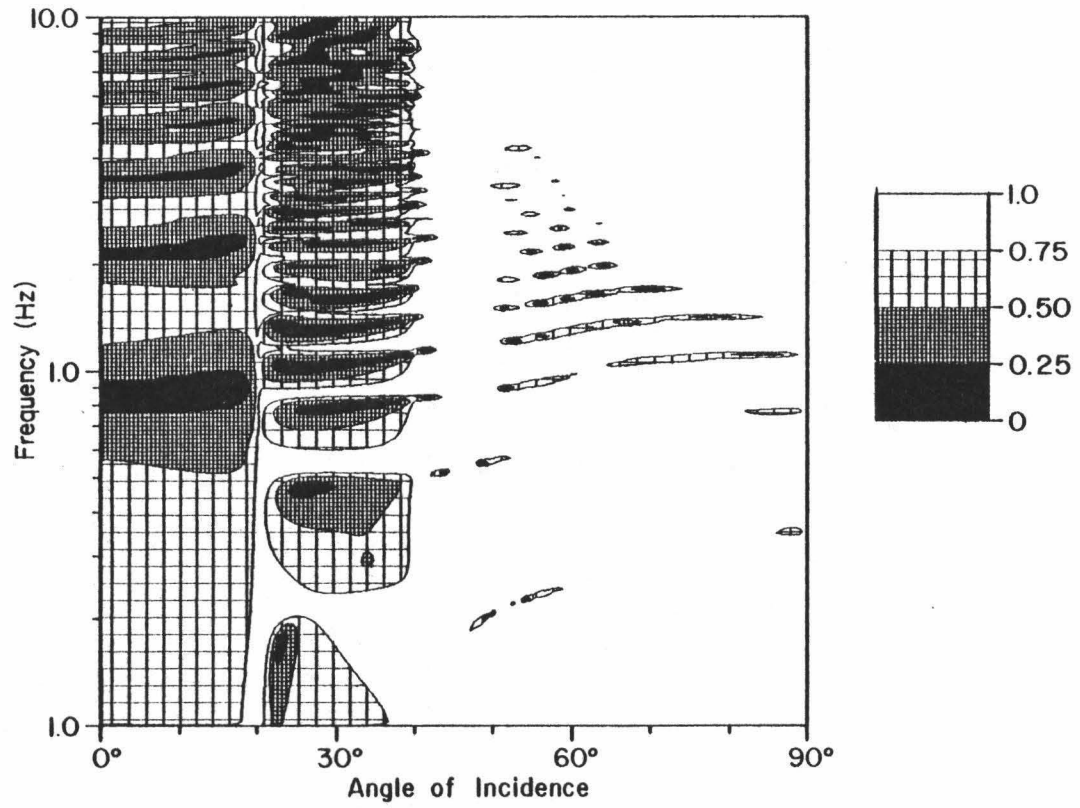


Figure 14. Modulus of the reflectivity function for Model 2.

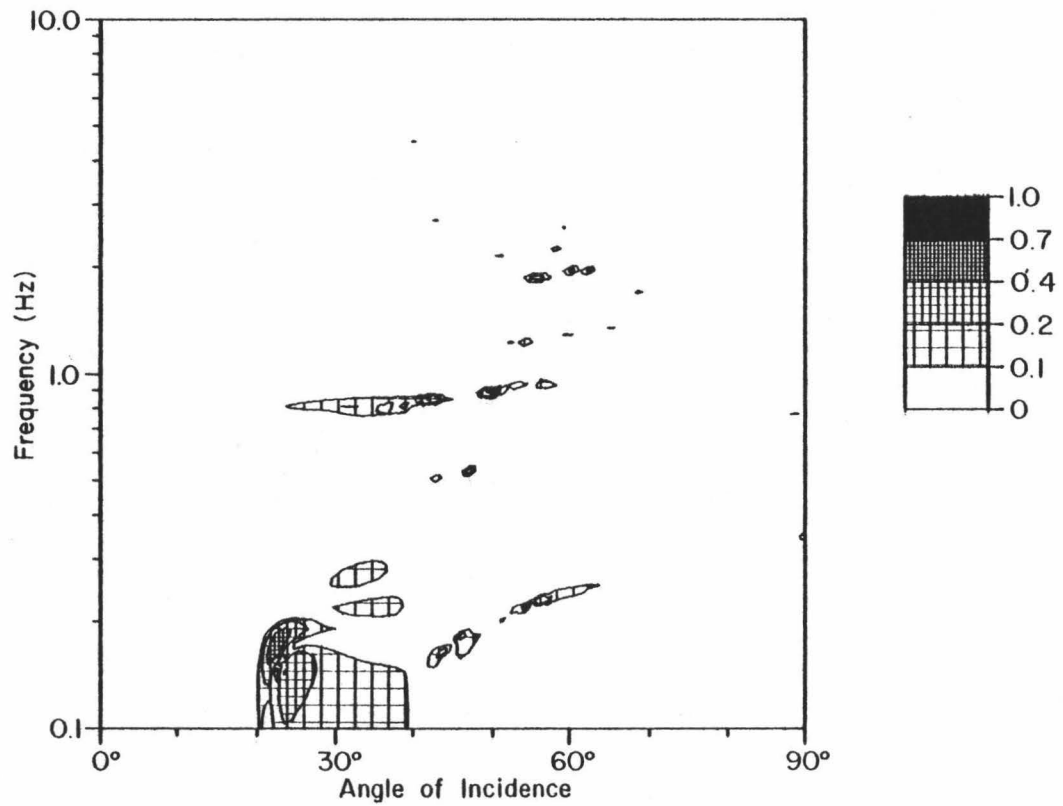


Figure 15. Error in the magnitude of the reflectivity for Model 2 if decoupling is assumed.

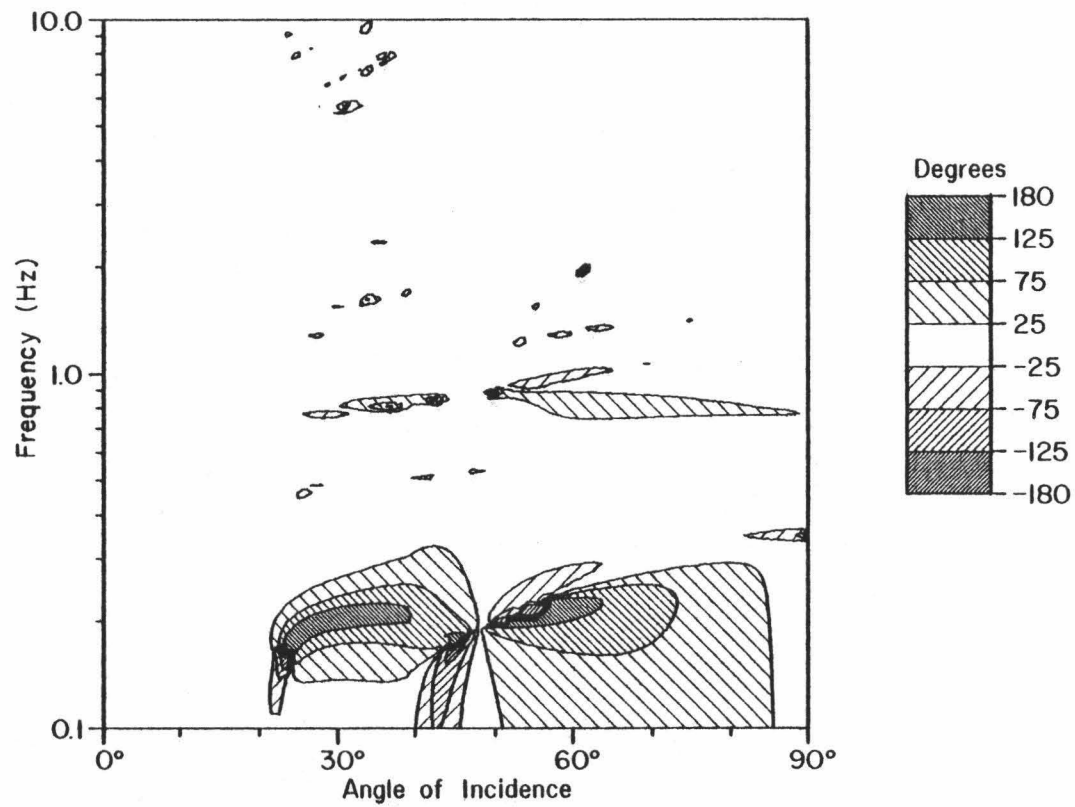


Figure 16. Error in the phase of the reflectivity for Model 2 if decoupling is assumed.

very similar to the results for Model 1 (Figs. 5 and 6) and the same conclusion can be drawn: Gradient-driven coupling can be ignored above 1 Hz. In retrospect this result is not surprising. As shown for Model 1, the most important effect of coupling appears to be the conversion of shear to compressional motion. The shear motion generated at the sediment-water interface by incident compressional waves in the water is refracted towards the normal because of the low shear velocity. To increase the shear velocity gradient (and hence coupling) in Model 2, the initial shear velocity had to be dropped, so the shear energy for Model 2 is refracted even more towards the normal. However, the degree of gradient-induced coupling is dependent on the angle between the propagation direction and the direction of variation of velocity. If this angle is small (normal incidence), coupling is negligible. The net result is that despite the greater shear gradient of Model 2, coupling is no greater than for Model 1. It is also apparent that gradient-driven coupling is largely independent of the attenuation structure.

C. Effects of Sediment Thickness

The most important effect of coupling is apparently to convert S to P motion. Because of the impedance contrasts, the generation of S motion by incident P waves is more efficient at the sediment-basement than the water-sediment interface. In thick sediments little P energy impinges on basement so conversion to shear is usually small. For

this reason the effect of sediment rigidity is much more pronounced in a thin sedimentary sequence than a thick one (Vidmar, 1980). It is therefore possible that gradient-driven coupling too would be more pronounced in a thin sequence. To investigate the effects of sediment thickness, the coupling analysis for Model 2 was repeated with the lower 530m of sediments removed, giving a total sediment thickness of 120m. The results are shown in Figures 17 and 18. As for the thicker sequence, gradient-driven coupling is minimal above 1 Hz. Although reduced in amplitude, the frequency and angle dependence of the coupling are almost identical to those for the thicker sequence except that they are displaced to higher frequency. This is best seen when comparing Figs. 16 and 18. If allowance is made for the logarithmic frequency scale the same basic pattern is apparent in both figures, but the pattern in Fig. 18 occurs at about 0.55 Hz higher frequency. Notice that the angular dependence of the coupling is unchanged, implying that for this structure Stoneley waves on the sediment-basement interface do not have an important effect on the coupling. For the thinner sequence, P waves first reach turnover within the sediments at an incidence angle of 66° rather than 48° , but this has no effect on the coupling as the angular dependence is unchanged.

That the same frequency and angle dependence appears for both thin and thick sequences implies that the coupling does indeed take place in the near-surface sediments where the gradients are the greatest. The thickness-dependent frequency shift is probably related to shear resonance in the sediments. For the structures investigated

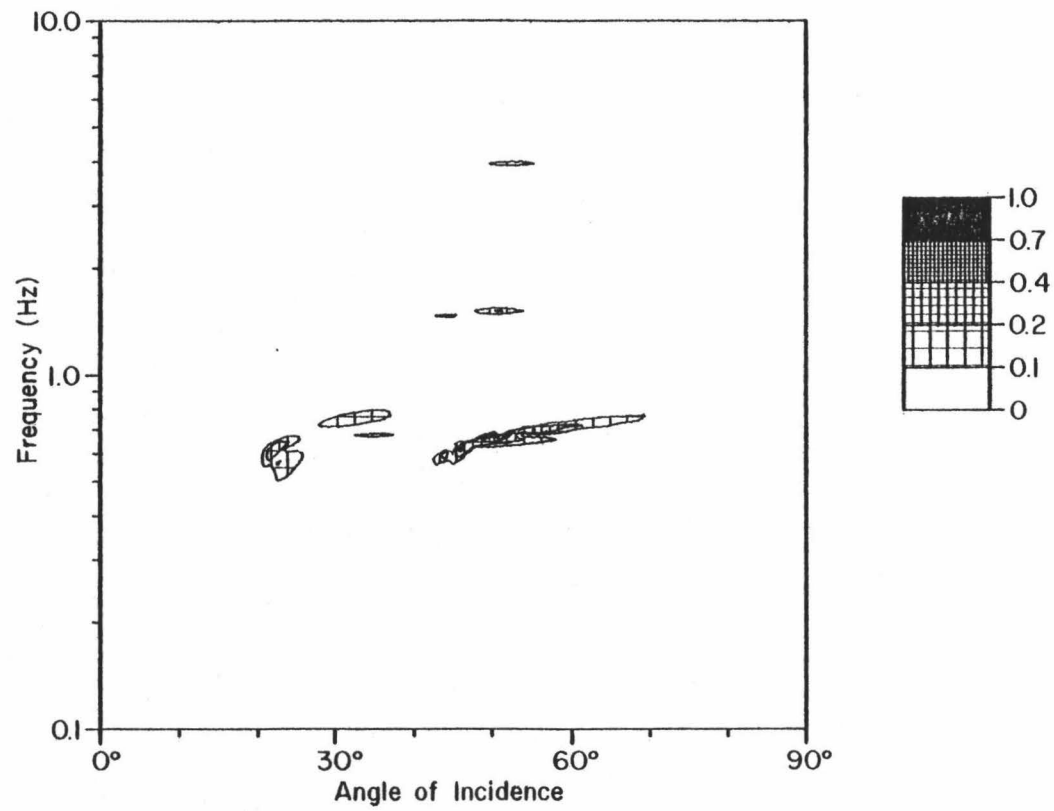


Figure 17. Magnitude error in the partial reflectivity for Model 2 if only the upper 120m of sediments are included.

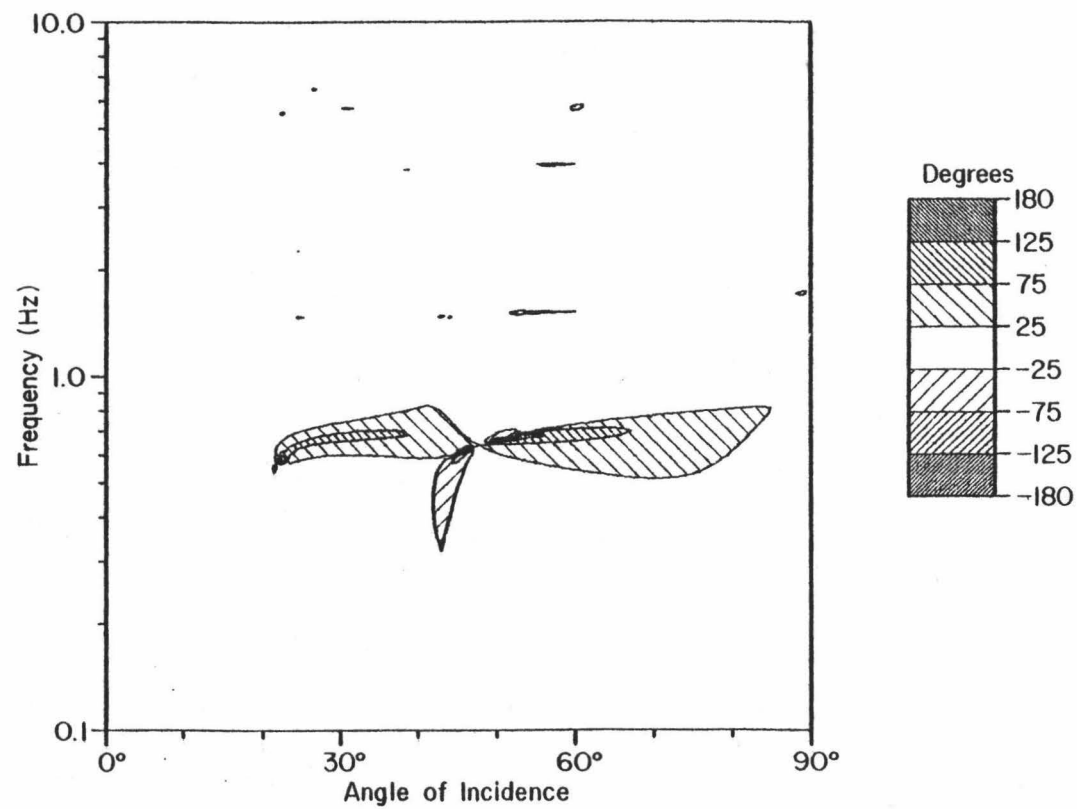


Figure 18. Phase error in the partial reflectivity for Model 2 if only the upper 120m of sediments are included.

here, no shear turnover occurs within the sediments for real angles of incidence so shear propagation involves the whole sediment column.

A final test of the thickness dependence was made with only the top 36m of sediments of Model 2 retained. The results were largely negative so they are not shown here. For such a very thin sequence the frequency shifting is so severe that the coupling peak occurs above the 1 Hz coupling threshold. No coupling of any importance occurs anywhere in ω - k space.

VI. DISCUSSION AND CONCLUSIONS

If complete solutions are required, the most efficient means of computing the acoustic response of an ocean bottom with arbitrary depth-dependence of elastic properties is to approximate that structure by homogeneous layers and use the classical Thomson-Haskell approach. Results not discussed here show further that the homogeneous layer approximation provides the most efficient means of obtaining complete solutions to any problem in body-wave seismology at frequencies above about 0.2 Hz. This does not mean, however, that this approach is the best way to solve the wave equation in any elastodynamic problem. Whenever high accuracy is required (as in surface wave dispersion studies) the Runge-Kutta approach would be superior.

Complete solutions are not always required or even warranted. For most problems the effects of gradient-driven coupling are so minor that it is not worth including coupling in the computation. These effects may be summarized as follows:

1. Coupling is only important below 1 Hz.
2. Coupling occurs as a consequence of the very high velocity gradients in near-surface sediments.
3. The frequency and intensity of the coupling maxima are dependent on sediment thickness and are probably controlled by the travel time of shear waves in the sediments.
4. The principal consequence of coupling, at least for the structures investigated here, is conversion of shear to compressional motion. As

a consequence the amplitude of shear arrivals is reduced and energy is added to the tails of compressional arrivals.

In practice, the subtleties introduced by coupling will probably be much less than the effects of uncertainties in the structure. This means that intrinsically expensive numerical solutions are either unnecessary or can be greatly simplified, and that the more efficient asymptotic approximations will probably prove adequate. Such approximations will not include the partial reflections from high velocity gradients that occur at low frequency (Chapman, 1980). Vidmar and Foreman (1979) estimate that such effects of gradients can be safely ignored only above 10 Hz, but that figure is probably rather conservative; the reflections are unlikely to be important above 3 Hz and as explained in the introduction, can probably be completely ignored. A simple and worthwhile assessment of the effects of partial reflections could be made by comparing the partial reflectivities as computed here with those obtained from an asymptotic approximation or from Vidmar and Foreman's numerical integration procedure.

This study does not provide enough justification for ignoring gradient-induced coupling completely. As more data on the physical properties of marine sediments become available (especially regarding the characteristics of shear-wave propagation), studies such as this should be repeated to verify that the decoupled reflectivity is adequate. One phenomenon which should be considered in such studies is anisotropy. It is well known that marine sediments can exhibit a strong transverse anisotropy (Bachman, 1979) and this will lead to P-SV coupling. Sprenke and Kanasewich (1977) have already devised a

convenient scheme for including transverse anisotropy in the homogeneous layer approximation. It is possible that the effects of strong velocity gradients and transverse anisotropy will combine to give an appreciable amount of continuous P-S coupling. This should be investigated.

A further phenomenon which should eventually be considered is frequency dependence of Q . A constant Q (or equivalently a linear relationship between attenuation and frequency) violates causality (Strick, 1967) and does not agree with experimental data on attenuation in sediments (Stoll, 1979). To include frequency dependence of Q in the Thomson-Haskell formalism is straightforward (O'Neill and Hill, 1979). Unfortunately, data on the exact nature of the frequency dependence are poor, especially at low frequencies, so an assessment of the effects of frequency-dependent Q must await a later study. It is unlikely that such frequency dependence will effect the conclusions of this work regarding P-S coupling.

REFERENCES

- Abo-Zena, A., 1979, Dispersion function computations for unlimited frequency values, *Geophys. J. R. Astron. Soc.*, v. 58, p. 91-105.
- Bachman, R.T., 1979, Acoustic anisotropy in marine sediments and sedimentary rocks, *J. Geophys. Res.*, v. 84, p. 7661-7663.
- Birchoff, G., 1937, On product integration, *J. Math. and Physics*, v. 16, p. 104-132.
- Chapman, C.H., 1974, The turning point of elastodynamic waves, *Geophys. J. R. Astron. Soc.*, v. 39, p. 613-621.
- Chapman, C.H., 1978, A new method for computing synthetic seismograms, *Geophys. J. R. Astron. Soc.*, v. 54, p. 481-518.
- Chapman, C.H., 1980, Long period corrections to body waves: theory, submitted to *Geophys. J. R. Astron. Soc.*
- Chapman, C.H., and R.A. Phinney, 1972, Diffracted seismic signals and their numerical solution, in Methods in computational physics, v. 12, B.A. Bolt, ed., Academic Press, New York, p. 165-230.
- Davis, D., 1965, Dispersed Stoneley waves on the ocean bottom, *Bull. Seismol. Soc. Am.*, v. 55, p. 903-918.
- Dunkin, J.W., 1965, Computation of modal solutions in layered elastic media at high frequencies, *Bull. Seismol. Soc. Am.*, v. 55, p. 335-358.
- Forsythe, G.E., M.A. Malcolm and C.B. Moler, 1977, Computer methods for mathematical computations, Prentice-Hall, Englewood Cliffs, N.J.
- Frisk, G.V., 1979, Inhomogeneous waves and the plane-wave reflection coefficient, *J. Acoust. Soc. Am.*, v. 66, p. 219-234.
- Fryer, G.J., 1978, Reflectivity of the ocean bottom at low frequency, *J. Acoust. Soc. Am.*, v. 63, p. 35-42.
- Fryer, G.J., 1980, A slowness approach to the reflectivity method of seismogram synthesis, *Geophys. J. R. Astron. Soc.*, in press.
- Fuchs, K., 1968, Das Reflexions- und Transmissionsvermögen eines geschichteten Mediums mit beliebiger Tiefenverteilung der elastischen Moduln und der Dichte für schragen Einfall ebener Wellen, *Zeit. Geophys.*, v. 34, p. 389-413.
- Gear, C.W., 1971, Numerical initial value problems in ordinary differential equations, Prentice-Hall, Englewood Cliffs, N.J.

- Gilbert, F. and G.E. Backus, 1966, Propagator matrices in elastic wave and vibration problems, *Geophysics*, v. 31, p. 326-332.
- Gupta, R.N., 1966a, Reflection of elastic waves from a linear transition layer, *Bull. Seismol. Soc. Am.*, v. 56, p. 511-526.
- Gupta, R.N., 1966b, Reflection of plane elastic waves from transition layers with arbitrary variation of velocity and density, *Bull. Seismol. Soc. Am.*, v. 56, p. 633-642.
- Hamilton, E.L., 1976a, Sound attenuation as a function of depth in the sea floor, *J. Acoust. Soc. Am.*, v. 59, p. 528-535.
- Hamilton, E.L., 1976b, Attenuation of shear waves in marine sediments, *J. Acoust. Soc. Am.*, v. 60, p. 334-338.
- Hamilton, E.L., 1978, Sound velocity-density relations in sea-floor sediments and rocks, *J. Acoust. Soc. Am.*, v. 63, p. 366-377.
- Hamilton, E.L., 1979a, Sound velocity gradients in marine sediments, *J. Acoust. Soc. Am.*, v. 65, p. 909-922.
- Hamilton, E.L., 1979b, V_p/V_s and Poisson's ratios in marine sediments and rocks, *J. Acoust. Soc. Am.*, v. 66, p. 1093-1101.
- Haskell, N., 1953. The dispersion of surface waves on multilayered media, *Bull. Seismol. Soc. Am.*, v. 43, p. 17-34.
- Hawker, K.E., 1978, Influence of Stoneley waves on plane-wave reflection coefficients: Characteristics of bottom reflection loss, *J. Acoust. Soc. Am.*, v. 64, p. 548-555.
- Helmberger, D.V., G. Engen and P. Scott, 1979, A note on velocity, density and attenuation models for marine sediments from multibounce phases, *J. Geophys. Res.*, v. 84, p. 667-671.
- Kennett, B.L.N., 1974, Reflections, rays and reverberations, *Bull. Seism. Soc. Am.*, v. 64, p. 1685-1696.
- Kennett, B.L.N., N.J. Kerry and J.H. Woodhouse, 1978, Symmetries in the reflection and transmission of elastic waves, *Geophys. J. R. Astron. Soc.*, v. 52, p. 215-229.
- Kind, R., 1976, Computation of reflection coefficients for layered media, *J. Geophys.*, v. 42, p. 191-200.
- Mitchell, S.K., and K.C. Focke, 1980, New measurements of compressional wave attenuation in deep ocean sediments, submitted to *J. Acoust. Soc. Am.*

- Mitchell, S.K., and J.J. Lemmon, 1979, A ray theory model of acoustic interaction with the ocean bottom, *J. Acoust. Soc. Am.*, v. 66, p. 855-861.
- Molotkov, L.A., V. Cerveny and O. Novotny, 1976, Low-frequency and high-frequency expressions for the reflection and transmission coefficients of seismic waves for transition layers, *Studia Geophys. et Geod.*, v. 20, p. 219-235.
- O'Neill, M.E., and D.P. Hill, 1979, Causal absorption: Its effect on synthetic seismograms computed by the reflectivity method, *Bull. Seism. Soc. Am.*, v. 69, p. 17-25.
- Pease, M.C., 1965, Methods in matrix algebra, Academic Press, New York.
- Pestel, E.C., and F.A. Leckie, 1963, Matrix methods in elastomechanics, McGraw-Hill, New York.
- Richards, P.G., 1971, Elastic wave solutions in stratified media, *Geophysics*, v. 36, p. 798-809.
- Richards, P.G., 1974, Weakly coupled potentials for high-frequency elastic waves in continuously stratified media, *Bull. Seismol. Soc. Am.*, v. 64, p. 1575-1588.
- Richards, P.G., 1976, On the adequacy of plane-wave reflection/transmission coefficients in the analysis of seismic body waves, *Bull. Seismol. Soc. Am.*, v. 66, p. 701-717.
- Santaniello, S.R., F.R. DiNapoli, R.K. Dullea and P.D. Herstein, 1979, Studies on the interaction of low-frequency acoustic signals with the ocean bottom, *Geophysics*, v. 44, p. 1922-1940.
- Shampine, L.F., and M.K. Gordon, 1975, Computer solution of ordinary differential equations, W.H. Freeman, San Francisco.
- Shampine, L.F., H.A. Watts and S.M. Davenport, 1976, Solving non-stiff ordinary differential equations - the state of the art, *SIAM (Soc. Ind. Appl. Math.) Rev.*, v. 18, p. 376-441.
- Shirley, D.J., and L.D. Hampton, 1978, Shear-wave measurements in laboratory sediments, *J. Acoust. Soc. Am.*, v. 63, p. 607-613.
- Sprenke, K.F., and E.R. Kanasewich, 1977, Synthetic seismograms and the response of an anisotropic attenuating medium, *Can. J. Earth. Sci.*, v. 14, p. 1062-1076.
- Stephen, R.A., 1977, Synthetic seismograms for the case of the receiver within the reflection zone, *Geophys. J. R. Astr. Soc.*, v. 51, p. 169-181.

- Stoll, R.D., 1979, Experimental studies of attenuation in sediments, J. Acoust. Soc. Am., v. 66, p. 1152-1160.
- Strick, E., 1967, The determination of Q, dynamic viscosity, and transient creep curves from wave propagation measurements, Geophys. J. R. Astron. Soc., v. 13, p. 197-218.
- Takeuchi, H., and M. Saito, 1972, Seismic surface waves, in Methods in computational physics, v. 11, B.A. Bolt, ed., Academic Press, New York, p. 217-295.
- Thomson, W.T., 1950, Transmission of elastic waves through a stratified solid medium, J. Appl. Phys., v. 21, p. 89-93.
- Vidmar, P.J., 1980, The effect of sediment rigidity on bottom reflection loss in a typical deep sea sediment, submitted to J. Acoust. Soc. Am.
- Vidmar, P.J., and T.L. Foreman, 1979, A plane wave reflection loss model including sediment rigidity, J. Acoust. Soc. Am., v. 66, p. 1830-1835.
- Volterra, V., 1887, Sulle equazioni differenziali lineari, Rendiconti dell'Accademia dei Lincei, series 4, v. 3, p. 393-396.
- Watson, T.H., 1970, A note on fast computation of Rayleigh wave dispersion in the multilayered elastic half-space, Bull. Seismol. Soc. Am., v. 60, p. 161-166.

APPENDIX A

REFLECTIVITY OF THE OCEAN BOTTOM AT LOW FREQUENCY

A paper published in the Journal of the Acoustical Society
of America, v. 63, p. 35-42 (January, 1978).

Reflectivity of the ocean bottom at low frequency^{a)}

Gerard J. Fryer

Hawaii Institute of Geophysics, 2525 Correa Road, Honolulu, Hawaii 96822
(Received 21 June 1977; revised 12 September 1977)

The theoretical reflectivity of the ocean bottom estimated from a model composed of fluid sediment layers is misleading because the effects of shear propagation are ignored. Reflectivity computations which include the effects of shear may be made using Thomson-Haskell matrix theory. The delta-matrix extension of this theory provides a method for computation of plane-wave reflectivity of a viscoelastic layered ocean bottom at the frequencies of interest in acoustics. The results from a hypothetical turbidite section show that when elastic parameters vary continuously with depth, conversion of compressional to shear energy is unimportant at frequencies above 20 Hz. However, at discontinuities, conversion to shear does occur. This strongly affects the reflectivity at all frequencies, except at small grazing angles and near-normal incidence.

PACS numbers: 43.30.Bp, 43.30.Dr

INTRODUCTION

Propagation of low-frequency acoustic waves in the ocean is complicated by interaction with the bottom structure. Acoustic waves in the water give rise to compressional, shear and interface waves within the bottom layering. These interactions become progressively more important as frequency is reduced because the acoustic disturbance then senses deeper and deeper structure. All such effects can be included in ray and normal mode analyses by making use of a complex plane-wave reflection coefficient R to characterize the ocean bottom.^{1,2}

Modeling the ocean bottom to calculate R theoretically is a complicated problem. Any realistic model must include layering, attenuation, and strong velocity and density gradients. The layering and velocity gradients introduce a further complication, conversion of compressional-(P) to shear-(SV)-wave motion. This will always occur at layer interfaces, but if velocity gradients are large, it will also occur continuously within a layer. In this case, compressional- and shear-wave propagations are coupled and cannot be regarded as distinct, the coupling becoming stronger as frequency is reduced.³ In marine sediments, compressional velocity gradients near the sediment surface⁴ are typically 1.3 s^{-1} , shear velocity gradients⁵ can be as high as 4.65 s^{-1} . Coupling can then be significant up to 10 Hz so its effect must be included in any computation of R at low frequency.

No theoretical studies of wave propagation in vertically heterogeneous media have been complete. Morris⁶ and Williams⁷ consider the ocean bottom to be a fluid with a pseudolinear increase in velocity with depth. This approach ignores P-to-SV conversion and does not allow variation of density or attenuation with depth within a layer. Gupta⁸ has derived a theory which includes shear propagation but it requires that shear and compressional velocity gradients be the same, a prop-

erty not exhibited by marine sediments.⁵ Richards⁹ and Richards and Frasier¹⁰ provide solutions which are applicable only to those cases for which phase velocity is higher than any layer velocity (i. e., turning points are ignored). It seems probable that a complete theory for wave propagation in vertically heterogeneous media will eventually be developed. The Langer approximation to a full wave theory¹¹ appears promising but as yet has not been extended to include P-SV coupling.

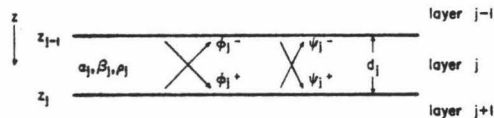
Until theoretical advances allow this wave-propagation problem to be solved, the simplest method to obtain acceptable solutions involving all interactions is the well-known Thomson-Haskell matrix method.^{12,13} In this method velocity and density gradients are approximated by many thin homogeneous layers. The chief objection to this technique is that the approximation is crude and the mathematical computation obscures the physics involved. These objections can be reduced somewhat by varying input parameters (for example, the thickness and number of layers) to see what effects these changes have on the final result. The Thomson-Haskell method does enjoy the advantage that it is readily adapted to any variation of elastic parameters with depth and can even be extended to include anisotropic effects¹⁴ although these will not be discussed here.

This paper describes the application of Thomson-Haskell theory to the determination of plane-wave reflection coefficients of the ocean bottom. Such an application has been described before by Bucker¹⁵ but he used a formulation of the theory which suffers inherent numerical problems. In this paper we take advantage of the reduced-delta matrix formulation of the theory which avoids these problems.

I. COMPUTATION OF REFLECTION COEFFICIENTS

It will be assumed here that the ocean bottom can be represented as a stack of $(n-1)$ homogeneous, isotropic, solid layers, separated by horizontal interfaces. The stack is sandwiched between a fluid half-space above (medium zero) and a solid half-space below (medium n). Velocity gradients are approximated by introducing many thin homogeneous layers into the stack, with P-SV conversions occurring only on reflection or refraction

^{a)}This work forms part of a doctoral dissertation at the University of Hawaii. Hawaii Institute of Geophysics contribution number 848.

FIG. 1. Potentials in layer j .

at interfaces. We wish to calculate the reflection coefficient, the ratio of reflected to incident sound pressure, for a plane monochromatic wave incident at a particular angle at the fluid–solid interface, i.e., we wish to find $R(\omega, k)$ where ω is angular frequency and k is horizontal wave number. The theory here follows Dunkin¹⁶ and Fuchs.¹⁷ In this section we ignore attenuative effects, in the next section these will be included by making the layers viscoelastic.

In the j th medium from the top of the stack we can define a potential vector of compressional (P) and shear (SV) displacement potentials.

$$\Phi_j(z) = [\phi_j^+(z), \psi_j^+(z), \phi_j^-(z), \psi_j^-(z)]^T, \quad (1)$$

where ϕ_j^+ , ψ_j^+ and ϕ_j^- , ψ_j^- represent P and SV potentials for waves traveling in the positive and negative z directions, as shown in Fig. 1. If we define a displacement-stress vector

$$s_j(z) = [u_j(z), w_j(z), \sigma_{xx}^{(j)}(z), \sigma_{xz}^{(j)}(z)]^T, \quad (2)$$

where u_j , w_j , $\sigma_{xx}^{(j)}$, $\sigma_{xz}^{(j)}$ represent horizontal and vertical displacement and normal and shear stress, respectively, then

$$s_j(z) = T_j \Phi_j(z). \quad (3)$$

Here T_j is a 4×4 matrix involving layer density ρ_j , the horizontal wave number k , and vertical wave numbers ν_j and ν_j' given by

$$\nu_j^2 = (\omega/\alpha_j)^2 - k^2, \quad \nu_j'^2 = (\omega/\beta_j)^2 - k^2, \quad (4)$$

where α_j , β_j are the P and S velocities, respectively.

The relationship between potentials at the top and bottom of layer j is

$$\Phi_j(z_j) = E_j \Phi_j(z_{j-1}), \quad (5)$$

where E_j is a 4×4 diagonal matrix with nonzero terms of the form $\exp(\pm i\nu_j d_j)$ and d_j is the layer thickness.

To obtain the potentials Φ_n of the lower half-space from the potentials Φ_0 in the upper half-space, Eqs. (3) and (5) are written for each layer and combined with the boundary conditions of continuity of displacements and stresses across each interface. If the upper half-space is solid, the final relationship is

$$\Phi_n(z_{n-1}) = M \Phi_0(z_0), \quad (6)$$

where

$$M = T_n^{-1} G_{n-1} G_{n-2} \dots G_2 G_1 T_0 \quad (7)$$

and the Haskell layer matrices, G_j , are defined by

$$G_j = T_j E_j T_j^{-1}. \quad (8)$$

Equation (6) cannot be used directly in the ocean-bottom case because when the shear velocity in medium zero is set equal to zero, the results become indeterminate. To accommodate a fluid upper half-space we use some of the results of Dunkin.¹⁶

In the fluid medium, since there is no shear wave propagation,

$$\Phi_0 = (\phi_0^+, 0, \phi_0^-, 0)^T \quad (9)$$

and T_0 takes on the simple form

$$T_0 = \begin{pmatrix} 0 & 0 & 0 & 0 \\ i\nu_0 & 0 & -i\nu_0 & 0 \\ -\rho_0\omega^2 & 0 & -\rho_0\omega^2 & 0 \\ 0 & 0 & 0 & 0 \end{pmatrix}. \quad (10)$$

At the interface z_0 between fluid and solid there is continuity of vertical displacement and normal stress, shear stress in the solid vanishes and horizontal displacement u_1 in the solid is unconstrained. These boundary conditions can be written

$$s_1(z_0) = T_0 \Phi_0(z_0) + \begin{pmatrix} u_1 \\ 0 \\ 0 \\ 0 \end{pmatrix}. \quad (11)$$

The potential vector in the lower half-space is then given by

$$\Phi_n(z_{n-1}) = M \Phi_0(z_0) + B \begin{pmatrix} u_1 \\ 0 \\ 0 \\ 0 \end{pmatrix}, \quad (12)$$

where

$$B = T_n^{-1} G_{n-1} G_{n-2} \dots G_2 G_1; \quad (13)$$

so

$$M = B T_0. \quad (14)$$

In the lower half-space there is no radiation coming from $z = \infty$ so

$$\Phi_n = (0, 0, \phi_n^+, \psi_n^+)^T. \quad (15)$$

Hence, using Eq. (9), the first two equations of Eq. (12) can be written

$$\begin{pmatrix} 0 \\ 0 \end{pmatrix} = \begin{pmatrix} m_{11} \\ m_{21} \end{pmatrix} \phi_0^+ + \begin{pmatrix} m_{13} \\ m_{23} \end{pmatrix} \phi_0^- + \begin{pmatrix} b_{11} \\ b_{21} \end{pmatrix} u_1, \quad (16)$$

where m_{ij} , b_{ij} are elements of the matrices M and B . Equation (16) may be rewritten

$$\begin{pmatrix} b_{11} & m_{11} \\ b_{21} & m_{21} \end{pmatrix} \begin{pmatrix} u \\ R \end{pmatrix} = - \begin{pmatrix} m_{13} \\ m_{23} \end{pmatrix}, \quad (17)$$

where $R = \phi_0^*/\phi_0^*$ is the desired reflection coefficient and $u = u_1/\phi_0^*$. From Eq. (17) we obtain the solution

$$R = (b_{21} m_{13} - b_{11} m_{23}) / (b_{11} m_{21} - b_{21} m_{11}). \quad (18)$$

B and M depend only on known material parameters and the specified frequency and wave number ω and k , so in theory $R(\omega, k)$ can be calculated.

II. ATTENUATION

To include effects of attenuation the simplest method is to make the propagation velocities or other elastic parameters complex.^{15,18,19} If the specific attenuation factor for compressional waves in layer j is $Q_{\alpha_j}^{-1}$, the complex P velocity $\alpha_j = \alpha_{Rj} + i\alpha_{Ij}$ is

$$\alpha_j = \alpha_{Rj}(1 + i/2Q_{\alpha_j}). \quad (19)$$

Here a time dependence of the form $\exp(+i\omega t)$ has been adopted (e.g., a wave traveling in the positive x direction would be represented by $\exp[i\omega(t - x/\alpha)]$). A similar expression to Eq. (19) can be written for shear waves. It is assumed here that Q is independent of frequency (i.e., that attenuation is directly proportional to frequency). This assumption appears to be approximately valid for both sediments and crystalline rocks^{20,21} at least within the frequency band of interest here (0.1–100 Hz). The near constancy of Q has some theoretical justification.²²

Introducing attenuation causes the plane waves to become inhomogeneous. To show this we consider the vector wave number

$$K = P - iA \quad (20)$$

with components

$$\begin{aligned} K_x &= k = P_x - iA_x, \\ K_z &= \nu = P_z - iA_z. \end{aligned} \quad (21)$$

In the fluid medium it is assumed that attenuation is negligible. The incident plane wave is homogeneous so k and $\nu = \nu_0$ [see Eq. (4)] are real in the fluid. As with elastic media, the boundary conditions for anelastic media demand that the horizontal wave number k be constant across an interface.²³ Hence if k is real in the liquid, it is everywhere real (and constant) so $A_x = 0$ everywhere.²⁴ The only nonzero component of the attenuation vector A is then A_z , so A is always vertical. In general the propagation vector P will not be vertical (except for normal incidence) so P and A will not be parallel and the plane waves will always be inhomogeneous within the layering. The physical characteristics of these waves, in contrast to those of homogeneous waves in purely elastic media, are described by Borchardt.²⁵ One useful consequence of wave propagation being inhomogeneous is that the concept of a critical angle is degraded. Instead of a discontinuous change from subcritical to supercritical reflection as the angle of incidence is varied, there is a rapid continuous one. This means that in modeling, for example, upward refraction of a wave in a region of velocity gradient, it is not necessary to have a great multiplicity of layers in the vicinity of the turnover depth.

Strictly, the implicit definition of Q in Eq. (19) is valid only for low-loss propagation of homogeneous waves. For sediments, the low-loss approximation is not valid and as we have seen, the plane waves in the layering are always inhomogeneous if there is any attenuation. However, since Q is in general very poorly known (particularly for shear waves in marine sediments), we assume that the errors incurred in using Eq. (19) are not significant. These errors would amount to at worst a 10% error in the imaginary part of the complex wave velocity. Q values are not known to this accuracy.

III. NUMERICAL DIFFICULTIES

Two numerical problems are inherent in the Thomson-Haskell method. These are loss of precision and exponent overflow, and are discussed in some detail by Dunkin¹⁶ and Schwab and Knopoff.²⁶ Both problems occur when the phase velocity $c = \omega/k$ is less than the propagation velocity in a layer. The wave then undergoes a supercritical reflection and the real parts of the exponents in matrix E of Eq. (5) become large. The loss of precision problem arises when large terms which should cancel in the final result fail to do so because of rounding error. One solution is to use the delta-matrix extension of Thomson-Haskell theory. The delta matrix \hat{G}_j of a 4×4 layer matrix G_j is the 6×6 matrix of all possible 2×2 subdeterminants of G_j .²⁷ In converting from G_j to \hat{G}_j , all the troublesome terms are eliminated analytically, so if delta matrices are used, matrix multiplications such as Eq. (13) can be performed without loss of precision. The delta matrices exhibit a degeneracy which allows actual computations to be performed using reduced 5×5 matrices.²⁸ Explicit expressions for delta-matrix elements are given by several authors.^{16,17,28,29}

To avoid the loss-of-precision problem, Eq. (18) should be reformulated in terms of delta matrices. Writing out the matrix equation $M = BT_0$ term by term and using Eq. (10), it can be readily shown that Eq. (18) reduces to the expression

$$R = (i\hat{B}_{11}\nu_0 + \hat{B}_{12}\rho_0\omega^2) / (i\hat{B}_{11}\nu_0 - \hat{B}_{12}\rho_0\omega^2), \quad (22)$$

where \hat{B}_{ij} are elements of the delta matrix \hat{B} of B . Note that only terms in the first row of \hat{B} are required, so only a single row needs to be carried through the multiplication of Eq. (13) if delta matrices are used. The same is true for solid media, only the first row of \hat{M} is needed to compute all reflectivities.²⁹ This means that delta matrices not only solve the loss-of-precision problem, they also speed computation. Kind²⁹ uses reduced delta matrices to compute the first row of \hat{M} and so obtain reflectivities for an all-solid, perfectly elastic structure. Since $\hat{M} = \hat{B}\hat{T}_0$, \hat{B} can be formed by truncating Kind's algorithm just before the last step. Naturally the program published by Kind has to be modified to accept complex velocities if attenuation is to be included.

The exponent overflow problem occurs for supercritical reflection at high frequency. The term $\exp(i\nu_j d_j)$ in the matrix E_j then becomes large and overflow occurs after a few matrix multiplications. The reflection coef-

TABLE I. Average Pacific crustal model.

Layer no.	Thickness (km)	P velocity (km/s ⁻¹)	S velocity (km/s ⁻¹)	Density (cgs)	Q _p	Q _s
0	—	1.5	0	1.03	∞	∞
1	0.5	2.08	0.4	1.97	150	15
2	0.95	4.46	2.4	2.46	500	193
3	1.15	6.00	3.4	2.71	500	214
4	1.7	6.74	3.8	2.87	700	296
5	2.9	7.47	4.2	3.08	700	296
6	∞	8.28	4.75	3.37	700	307

efficient is calculated by carrying a row vector through the matrix multiplications. Since the desired result, Eq. (22), is a ratio, the overflow problem is readily solved by normalizing this row vector to the magnitude of its largest element after each matrix multiplication. However, as wave number k is increased (by increasing frequency or lowering phase velocity), the exponents get so large that overflow occurs in calculating the elements of G_j . At still higher values of k , $|v_j d_j|$ gets so large that the complex exponential cannot be evaluated.

The solution is obvious once it is recognized that when $|v_j d_j|$ becomes large, very little energy penetrates layer j so the deeper structure can be ignored. This layer reduction technique is commonly used in surface-wave dispersion studies.²⁶ To determine if such layer reduction gives acceptable results, ocean floor reflection coefficients were calculated for a simplified crustal section of the Pacific Ocean. The structure used is shown in Table I. This structure was chosen because the high velocities and thick layers result in numerical problems at relatively low frequencies. Figure 2 shows the modulus of the reflectivity function between 22 and 32 Hz for a plane-wave incident at 20° from the vertical on the ocean bottom. The phase velocity of this disturbance is 4.39 km/s. Referring to Table I, this means that any P disturbance is supercritical for layer 2 and all deeper layers. Overflow occurred during P -wave computations for the basal crustal layer (layer 5) at a frequency of 26.2 Hz. This point is shown on Fig. 2. For all frequencies higher than 26.2 Hz, layer 5 was made the lower half-space and layer 6 was ignored. It is apparent from Fig. 2 that by removing the lowest

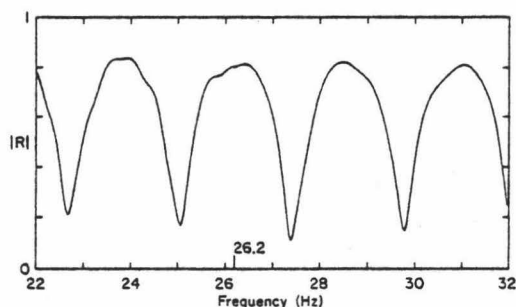


FIG. 2. Reflectivity of average Pacific crust for a plane wave at 20° angle of incidence on the ocean bottom. Overflow and layer reduction occurs at 26.2 Hz.

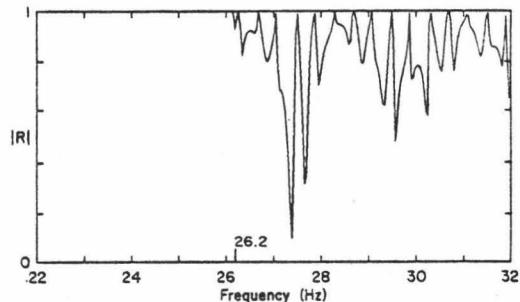


FIG. 3. Reflectivity of average Pacific crust for a plane wave incident at 20° on the ocean bottom computed ignoring attenuation. Overflow and layer reduction occurs at 26.2 Hz; results at higher frequencies are erroneous.

layer little information has been lost, the character of the reflectivity does not change as frequency increases through the overflow point.

It must be emphasized here that the layer reduction gave acceptable results only because a reasonable attenuation structure was included in the model. If Q_s , the quality factor for shear waves, is very large (or if there is no attenuation), shear waves penetrate to the mantle (layer 6) and are reflected. In this case there is an appreciable change in the character of the reflectivity if the lowest interface is ignored. This is shown in Fig. 3, computed for zero attenuation. Here the reflectivity is unity because all energy is supercritical at the half-space. At 26.2 Hz, where overflow occurs, the half-space is redefined. The shear wave velocity in the half-space is no longer higher than the phase velocity of the disturbance, so a complex reflectivity structure appears.

IV. TYPICAL RESULTS

Several analyses were run for an hypothetical turbidite section determined from data presented by Hamilton.^{4,5,20,30-32} Details of the model are shown in Table II. The model approximates the continuous variation of elastic parameters with depth by three zones in which variations are linear: 0-36, 36-120, and 120-650 m. Each zone is in turn approximated by a series of homogeneous layers. The high attenuation (low Q) of sediments reduces the necessity to use a large number of layers in the approximation. Only five layers are used for the 120-650-m zone, this appears to be sufficient to determine the gross features of the reflectivity function at frequencies below 50 Hz (doubling the number of layers did not materially affect the result). Because of the very sparse data on attenuation of shear waves, the quality factor for shear waves Q_s has been arbitrarily set at $Q_p/10$, following the recommendation of Hamilton.³² The turbidite section is underlain by basement at 650 m below the ocean bottom.

Reflectivities computed from the turbidite model are shown in Figs. 4-7; each figure shows the magnitude of the reflectivity $|R|$ as a function of frequency from 0.1 to 100 Hz, for a particular angle of incidence. At 10°

TABLE II. Model parameters.

Thickness (km)	Number of layers	P velocity (top) (km/s)	P-vel gradient (s ⁻¹)	S velocity (top) (km/s)	S-vel gradient (s ⁻¹)	Density (cgs)	Density gradient (km ⁻¹)	Q _a ^a (top)	Q _a gradient (km ⁻¹)
Turbidite Model									
—	1	1.53	0	0	0	1.03	0	∞	0
0.036	3	1.51	2.0	0.116	4.65	1.53	1.36	278	-2944
0.084	3	1.582	1.09	0.283	1.28	1.579	1.31	172	-1083
0.530	5	1.674	0.8	0.391	0.58	1.689	0.92	81	+50.9
∞	1	4.46	0	2.4	0	2.46	0	750	0
Modified Morris ^b Area A									
—	1	1.5449	0	0	0	1.051	0	∞	0
0.0046	5	1.53	1.0	0.12	4.35	1.4	0	25	0
0.100	15	1.5758	1.0	0.2	2.5	1.6	0	860	0
∞	1	4.46	0	2.4	0	2.46	0	750	0

^aIn both models $Q_s = Q_a/10$ in sediments, $Q_s = 290$ in lower half-space.

^bSee Ref. 6.

angle of incidence (Fig. 4), there is negligible conversion from compressional to shear energy. Shear is responsible for only minor changes in slope of the reflectivity function at frequencies below 2 Hz. The reflectivity peaks arise from interference within the structure, primarily from surface to basement reflections. Attenuation is unimportant, most of the energy is lost in the form of compressional waves escaping to the lower half-space.

At 30° (Fig. 5), conversion to shear, mainly on reflection from basement, explains all the structure below 1 Hz. This is confirmed by repeating the computation with vanishingly small shear velocity. Above 1 Hz, attenuation of shear waves is so high that the effect of shear decays until it appears only as a rapid oscillation superimposed on the background compressional reflection peaks. By 10 Hz the effect has died away completely. For an angle of incidence of 30°, compressional waves are supercritically reflected at the sediment-basement interface but shear waves are not, so conversion from *P* to *S* at the lowest interface is very efficient. Considerable energy over the whole frequency band is lost in the form of refracted shear

waves in the lower half-space; in the absence of this *P* to *S* conversion, the reflectivity would be everywhere larger by about 0.2.

At 50° (Fig. 6), conversion to shear (this time within the sediment column) is again responsible for the minima below 1 Hz but rapidly decays at higher frequencies and is negligible above 7 Hz. The very high value for reflectivity at low frequencies occurs because all disturbance (both *P* and *S*) is supercritical at the lower half-space and undergoes total reflection.

At 70° (Fig. 7), compressional waves are supercritical high in the sediment column, shear waves at the lowest interface. The strong absorption apparent below 3 Hz arises entirely from conversion to shear waves within the sediment column and the resulting high attenuation. If shear propagation were ignored the reflectivity function would decay slowly from near unity at 0.1 Hz to become continuous with the curve of Fig. 7 at about 3 Hz. Shear does not affect reflectivity above 3 Hz. The oscillation above 20 Hz is probably an interference phenomenon arising from compressional energy being refracted upwards in the sediments and reflected down-

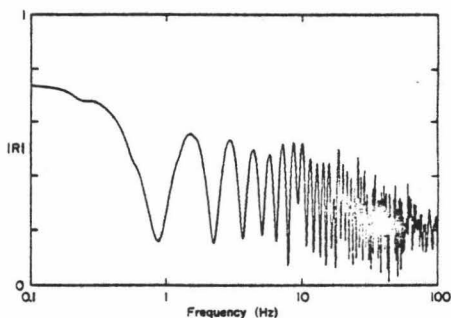


FIG. 4. Reflectivity computed for the turbidite model for a plane wave at 10° angle of incidence on the ocean bottom.

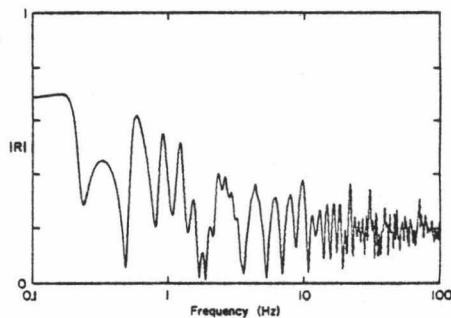


FIG. 5. Reflectivity computed for the turbidite model for a plane wave at 30° angle of incidence on the ocean bottom.

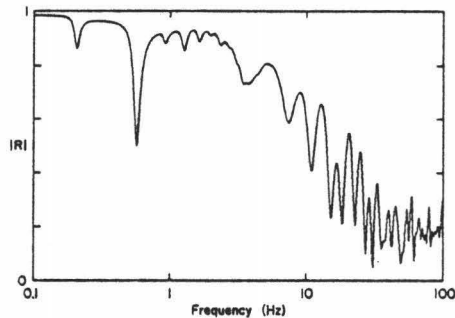


FIG. 6. Reflectivity computed for the turbidite model for a plane wave at 50° angle of incidence on the ocean bottom.

wards at the sediment-water interface. Removing the very minor low-velocity zone at the sediment-water interface (by increasing the surface sediment velocity) has negligible effect on this feature.

A more common method of presenting reflectivity information is in the form of bottom loss ($-20 \log_{10} |R|$) as a function of grazing angle (90° minus the angle of incidence) for a particular frequency. Figure 8 shows bottom loss at 20 Hz for the hypothetical turbidite section. The upper curve includes shear propagation effects, the lower curve was computed ignoring shear. Very low reflection loss occurs until the grazing angle reaches 20° . This is where energy begins to penetrate through the zone of very strong velocity and density gradients forming the first 36 m of sediments. Interference effects within the sediments give rise to absorption peaks between 20° and 40° ; similar interference is shown by Morris.⁶ Beyond 40° interaction with the basement becomes the predominant effect, shear conversion becomes important, and the two curves diverge. At 50° the critical angle for shear waves at the sediment-basement interface is reached so at large grazing angles there is considerable loss of energy in the form of shear waves in the lower half-space. The critical angle for compressional waves at the sediment-basement interface is reached at 70° , at larger angles

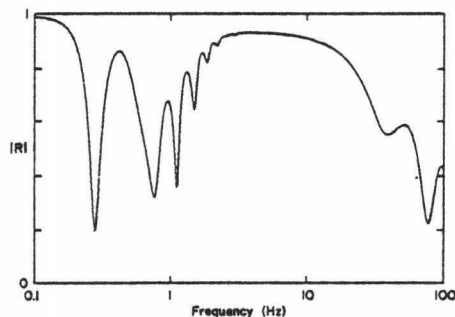


FIG. 7. Reflectivity computed for the turbidite model for a plane wave at 70° angle of incidence on the ocean bottom.

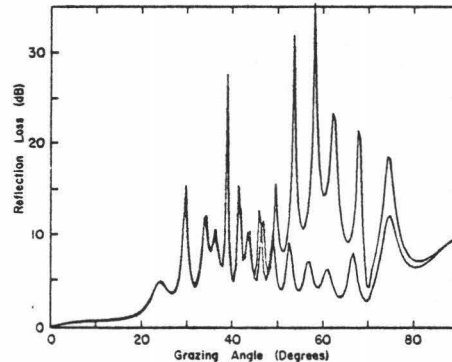


FIG. 8. Bottom reflection loss at 20 Hz for the turbidite model. The upper curve includes shear propagation effects, the lower curve does not.

the predominant energy loss is in the form of compressional waves in the lower half-space, so the shear and nonshear curves converge. In the real Earth, behavior at grazing angles greater than 50° would be modified by sub-basement structure.

Figure 9 shows bottom loss at 200 Hz calculated from the area A model of Morris.⁵ Results obtained from this model have been the subject of some discussion by Williams.⁷ This model consists of 4.6 m of silty clay with a 1-s^{-1} compressional velocity gradient overlying volcanic ash also with a gradient of 1 s^{-1} . Between clay and ash is a minor velocity discontinuity, a jump in compressional velocity of 0.0412 km/s. For the purposes of this study the ash layer was assumed to be 100 m thick (in Morris' work it was infinitely thick). Q for compressional waves was calculated from the attenuation coefficients provided by Morris, in the silty clay it was 25 and in the ash, 860. Shear velocity was inferred and shear Q was arbitrarily set at one tenth of the value for compressional waves. Complete details of the structure are shown in Table II.

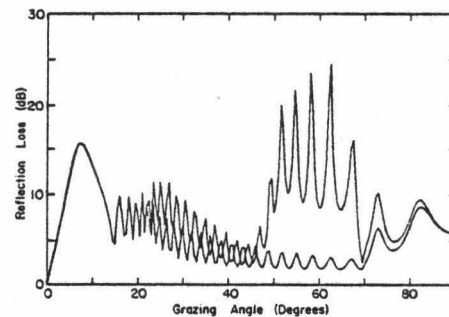


FIG. 9. Bottom reflection loss at 200 Hz for the modified Morris Area A model. The upper curve includes shear propagation effects, the lower curve does not.

As with Fig. 8, Fig. 9 shows results obtained both by including and ignoring shear. The same features as Fig. 2 of Morris are apparent for grazing angles less than 20° . Beyond this angle compressional waves penetrate to the basement and are reflected, giving lower bottom loss than the Morris model in which the basement is absent. Some compressional energy is converted to shear on reflection, explaining the separation of the two curves. For grazing angles greater than 50° , Fig. 9 shows the same separation between shear and nonshear curves as Fig. 8. The cause is the same, energy being carried off by shear waves escaping into the lower half-space. To reduce the height of the large bottom-loss peaks beyond 50° to satisfy the experimental data of Morris (Ref. 6, Fig. 2), the model parameters would have to be adjusted. Attenuation in the ash layer would have to be increased; the value of 860 for Q , based on attenuation of 0.004 dB/m at 200 Hz seems too large. To reduce the oscillations in the theoretical curve between 15° and 50° , the ash layer would have to be thinned. Reducing the ash layer thickness to 15 m and Q_a to 100 gives reasonable agreement with the data. No doubt other models would also give acceptable results.

V. DISCUSSION AND CONCLUSIONS

The reduced delta-matrix formulation of Thomson-Haskell theory is readily applicable to the problem of determining ocean-floor reflectivity. The technique may be used (with some inconvenience in terms of computation time and model complexity) to handle the case of continuous vertical variation of elastic parameters. Despite the philosophical objections to the large amount of computation involved, the technique is attractive since any arbitrary depth dependence of any parameter can be modelled. However the Thomson-Haskell method requires crude approximation (homogeneous layers) and is only used for lack of a more satisfactory theory.

The analyses discussed here indicate that even in the presence of high velocity gradients, compressional to shear conversion within the sediment column appears to be unimportant above 20 Hz. This is true only in the absence of discontinuities, conversion to shear would be important if strong contrasts in elastic parameters existed in the column (i.e., at erosional unconformities). If any energy impinges on the sediment basement interface (or deeper interfaces), conversion to shear is important at all frequencies and must be included in the analysis.

ACKNOWLEDGMENTS

I should like to thank Mark Odegard and George Sutton of Hawaii Institute of Geophysics for their critical reviews. This work was supported by the Ocean Science and Technology Division of the Office of Naval Research.

¹H. P. Bucker, "Sound Propagation in a Channel with Lossy Boundaries," *J. Acoust. Soc. Am.* 48, 1187-1194 (1970).

²H. P. Bucker, "Sound Propagation Calculations Using Bottom Reflection Functions," in *Physics of Sound in Marine Sedi-*

ments, edited by Lloyd Hampton (Plenum, New York, 1974), pp. 223-239.

³P. G. Richards, "Weakly Coupled Potentials for High-frequency Elastic Waves in Continuously Stratified Media," *Bull. Seismol. Soc. Am.* 64, 1575-1588 (1974).

⁴E. L. Hamilton, D. G. Moore, E. C. Buffington, P. L. Sherer, and J. R. Curray, "Sediment Velocities from Sonobuoys: Bay of Bengal, Bering Sea, Japan Sea, and North Pacific," *J. Geophys. Res.* 79, 2653-2668 (1974).

⁵E. L. Hamilton, "Shear-Wave Velocity Versus Depth in Marine Sediments: A Review," *Geophysics* 41, 985-996 (1976).

⁶H. E. Morris, "Bottom-Reflection-Loss Model with a Velocity Gradient," *J. Acoust. Soc. Am.* 48, 1198-1202 (1970).

⁷A. O. Williams, Jr., "Acoustic Reflection From a Structured Sea Bottom," *J. Acoust. Soc. Am.* 59, 62-68 (1976).

⁸R. N. Gupta, "Reflection of Elastic Waves from a Linear Transition Layer," *Bull. Seismol. Soc. Am.* 56, 511-526 (1966).

⁹P. G. Richards, "Elastic Wave Solutions in Stratified Media," *Geophysics* 36, 798-809 (1971).

¹⁰P. G. Richards and C. W. Frasier, "Scattering of Elastic Waves from Depth-Dependent Inhomogeneities," *Geophysics* 41, 441-458 (1976).

¹¹P. G. Richards, "On the Adequacy of Plane-Wave Reflection/Transmission Coefficients in the Analysis of Seismic Body Waves," *Bull. Seismol. Soc. Am.* 66, 701-717 (1976).

¹²W. T. Thomson, "Transmission of Elastic Waves Through a Stratified Solid Medium," *J. Appl. Phys.* 21, 89-93 (1950).

¹³N. A. Haskell, "The Dispersion of Surface Waves on Multilayered Media," *Bull. Seismol. Soc. Am.* 43, 17-34 (1953).

¹⁴S. Crampin, "The Dispersion of Surface Waves in Multilayered Anisotropic Media," *Geophys. J. R. Astron. Soc.* 21, 387-402 (1970).

¹⁵H. P. Bucker, J. A. Whitney, G. S. Yee, and R. R. Gardner, "Reflection of Low-Frequency Sonar Signals from a Smooth Ocean Bottom," *J. Acoust. Soc. Am.* 37, 1037-1051 (1965).

¹⁶J. W. Dunkin, "Computation of Modal Solutions in Layered, Elastic Media at High Frequencies," *Bull. Seismol. Soc. Am.* 55, 335-358 (1965).

¹⁷K. Fuchs, "Das Reflexions- und Transmissionsvermögen eines geschichteten Mediums mit beliebiger Tiefen-Verteilung der elastischen Moduln und der Dichte für schrägen Einfall ebener Wellen," *Z. Geophys.* 34, 389-413 (1968).

¹⁸F. A. Schwab and L. Knopoff, "Fast Surface Wave and Free Mode Computations," in *Methods in Computational Physics*, edited by B. A. Bolt (Academic, New York, 1972), Vol. 11, pp. 146-148.

¹⁹B. L. N. Kennett, "The Effects of Attenuation on Seismograms," *Bull. Seismol. Soc. Am.* 65, 1643-1651 (1975).

²⁰E. L. Hamilton, "Sound Attenuation as a Function of Depth in the Sea Floor," *J. Acoust. Soc. Am.* 59, 528-535 (1976).

²¹P. B. Attewell and Y. V. Ramana, "Wave Attenuation and Internal Friction as Functions of Frequency in Rocks," *Geophysics* 31, 1049-1056 (1966).

²²H.-P. Liu, D. L. Anderson, and H. Kanamori, "Velocity Dispersion due to Anelasticity: Implications for Seismology and Mantle Composition," *Geophys. J. R. Astron. Soc.* 47, 41-58 (1976).

²³R. D. Borchardt, "Reflection and Refraction of P and Type-I S Waves at Plane Interfaces in Elastic and Anelastic Media," *Bull. Seismol. Soc. Am.* (in press).

²⁴W. Silva, "Body Waves in a Layered Anelastic Solid," *Bull. Seismol. Soc. Am.* 66, 1539-1554 (1976).

²⁵R. D. Borchardt, "Energy and Plane Waves in Linear Viscoelastic Media," *J. Geophys. Res.* 78, 2442-2453 (1973).

²⁶F. Schwab and L. Knopoff, "Surface Wave Dispersion Computations," *Bull. Seismol. Soc. Am.* 60, 321-344 (1970).

²⁷E. C. Pestel and F. A. Leckie, *Matrix Methods in Elastomechanics* (McGraw-Hill, New York, 1963), Chap. 7, pp. 194-197.

- ²⁸T. H. Watson. "A Note on Fast Computation of Rayleigh Wave Dispersion in the Multilayered Elastic Half-Space," *Bull. Seismol. Soc. Am.* 60, 161-166 (1970).
- ²⁹R. Kind. "Computation of Reflection Coefficients for Layered Media." *J. Geophys.* 47, 41-58 (1976).
- ³⁰E. L. Hamilton. "Compressional-Wave Attenuation in Marine Sediments." *Geophysics* 37, 620-646 (1972).
- ³¹E. L. Hamilton. "Variations of Density and Porosity with Depth in Deep-Sea Sediments," *J. Sediment. Petrol.* 46, 280-300 (1976).
- ³²E. L. Hamilton. "Attenuation of Shear Waves in Marine Sediments," *J. Acoust. Soc. Am.* 60, 334-338 (1976).

APPENDIX B

A SLOWNESS APPROACH TO THE REFLECTIVITY METHOD OF
SEISMOGRAM SYNTHESIS

Preprint of a paper submitted to the Geophysical Journal
of the Royal Astronomical Society (December, 1979).

A slowness approach to the reflectivity method of seismogram synthesis

Gerard J. Fryer

Hawaii Institute of Geophysics, 2525 Correa Road, Honolulu,
Hawaii 96822, USA

Short title: Reflectivity-slowness synthetics

Summary. Of the many schemes available for computing synthetic seismograms, the reflectivity method is probably the most widely used because of its ability to provide complete solutions. The method does, however, suffer the disadvantage that intermediate results are quite difficult to interpret. A new reflectivity technique, here called reflectivity-slowness, results if the original method is reformulated using a slowness rather than a spectral approach. The new procedure bears a strong similarity to the WKBJ method, but retains the ability to give complete solutions. The reflectivity-slowness and WKBJ methods share the property that intermediate results are readily interpreted; this feature may eventually be exploited in the solution of the inverse problem.

Introduction

The reflectivity method for the computation of synthetic seismograms (Fuchs & Müller 1971) is widely used as an aid to the interpretation of body-wave seismograms, especially in lithospheric studies. The method does, however, suffer two major disadvantages. The first is expense. The technique involves the computation of a reflectivity function and the double transformation of that function from frequency-wavenumber to time-distance space. The reflectivity function must be adequately sampled to avoid aliasing on transformation, so that a very large number of reflectivity computations are required. Determination of reflectivities involves solution of a differential equation for the depth-dependent part of the wave equation, which, even for very simple problems, implies numerical solution. The transforms too are evaluated numerically, so every stage of the synthesis is inherently expensive. The second disadvantage is more profound. The early recourse to numerical analysis means that intermediate results are complicated and difficult to interpret. Since synthetics are used primarily as a guide to the solution of the inverse problem, this complication is unfortunate; it forces model improvements to be made essentially by trial error. One method for the computation of theoretical seismograms does not suffer the problem of complexity or expense: the WKBJ method (Chapman 1978, Dey-Sarkar & Chapman 1978). The WKBJ method is approximate, however, so it is most useful for the initial iterations of an inversion process. Because it is the most exact of the methods available, the reflectivity method should be used to verify the final models, especially if structures are complicated by high velocity gradients or low velocity zones (Burdick & Orcutt 1979). Any

reformulation of the reflectivity technique which would reduce expense or allow a simpler interpretation of intermediate results would obviously be worthwhile.

Any seismogram synthesis technique involves operations equivalent to those in the reflectivity method: solution of a differential equation followed by two inverse transformations which are essentially an integration with respect to frequency and one with respect to wavenumber (or equivalently to waveslowness). The two transformations may be performed in either order separating synthesis techniques into the two classes identified by Chapman (1978). A spectral method is one in which the waveslowness integral is evaluated first; the alternative, initial evaluation of the frequency integral, is called a slowness method. The reflectivity method is the best known of the spectral methods, but it can be reformulated using the slowness approach. That reformulation is the subject of this paper. I shall refer to the reformulated technique as the reflectivity-slowness method and illustrate its use by considering a simple example. It will become apparent that the chief advantage of the new method is that intermediate results are much simpler to interpret.

General Theory

The reflectivity method of Fuchs & Müller (1971) is a scheme for computing the response of a layered half-space to a near-surface point source. In order to reduce computation time the complete response is computed only for the lower part of the structure, called the "reflection zone." For shallower layers (which are of lesser interest), only transmission losses and time delays are considered. We shall use the same

approach here, but for simplicity we shall consider only a single fluid (ocean) layer overlying the reflection zone. For more complicated shallow structures the generalizations of Fuchs & Müller (1971) and Kennett (1975) may readily be incorporated into this method.

The geometry of the problem is shown in Fig. 1. The structure consists of a water layer of depth h and uniform sound velocity α_0 . The reflection zone begins at the ocean bottom and includes all deeper structure. We consider a receiver at a depth z from the surface a horizontal distance r from an explosive source with a displacement potential time function $s(t)$. The Fourier transformed displacement potential for energy returned from the ocean bottom (i.e. from the reflection zone) will be

$$\hat{\phi}(r, z, \omega) = \hat{s}(\omega) \int_0^{\infty} (k/i\nu_0) R_{pp}(\omega, k) J_0(kr) \exp\{i\nu_0(2h-z)\} dk, \quad (1)$$

where R_{pp} is the P-P reflection at the ocean bottom, k is the horizontal wavenumber and ν_0 is the vertical wavenumber in the water (medium zero) given by

$$\nu_0^2 = (\omega/\alpha_0)^2 - k^2.$$

The reflectivity function R_{pp} includes all multiple reflections and inter-conversions of wave types within the reflection zone. It is usually computed using one of the more efficient matrix methods such as the phase-related approach of Kennett (1974).

Equation (1) is consistent with the following definition of the Fourier transform pair:

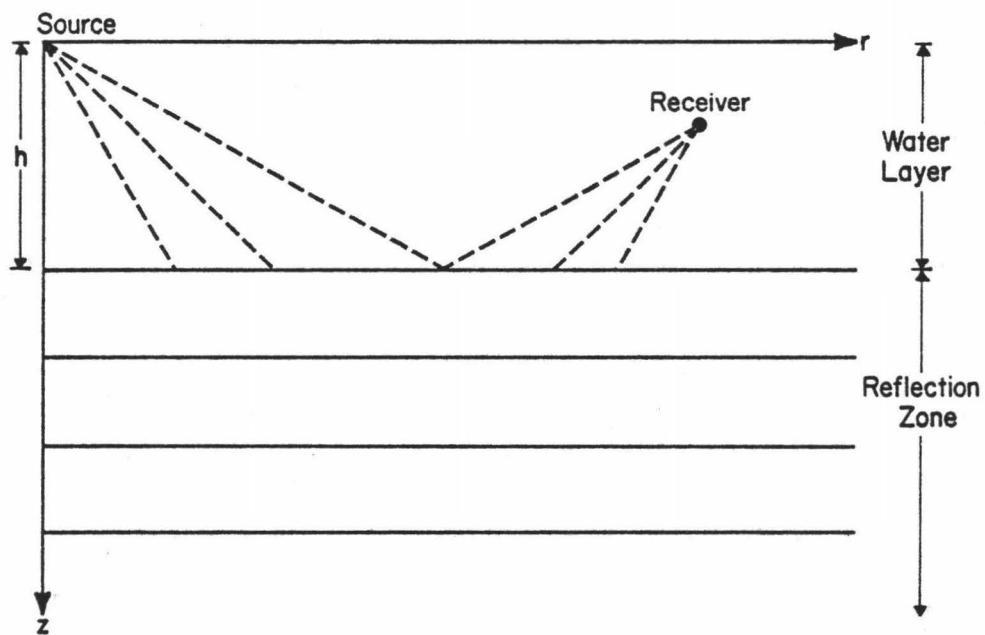


Figure 1. The problem considered. The response of a layered half-space (the reflection zone) to a point source at the surface of an overlying water layer is to be synthesized. Direct and surface reflected phases are ignored.

$$\hat{\phi}(\omega) = \int_{-\infty}^{\infty} \phi(t) e^{i\omega t} dt,$$

$$\phi(t) = \frac{1}{2\pi} \int_{-\infty}^{\infty} \hat{\phi}(\omega) e^{-i\omega t} d\omega.$$

As Chapman (1978), we have denoted the Fourier transform of $\phi(t)$ by $\hat{\phi}(\omega)$.

From equation (1) the vertical displacement, w , is obtained by taking the derivative with respect to depth z . This gives

$$\hat{w}(r, z, \omega) = -\hat{s}(\omega) \int_0^{\infty} R_{pp}(\omega, k) J_0(kr) \exp\{i v_0(2h-z)\} k dk.$$

Making the substitution $k=\omega p$ we obtain the slowness integral

$$\hat{w}(r, z, \omega) = -\hat{s}(\omega) \int_0^{\infty} R_{pp}(\omega, p) J_0(\omega p r) \exp\{i v_0(2h-z)\} \omega^2 p dp, \quad (2)$$

where p is the horizontal slowness and q is the vertical slowness given by

$$q^2 = \alpha_0^{-2} - p^2.$$

The desired time function is the inverse Fourier transform of equation (2)

$$\hat{w}(r, z, t) = -\frac{1}{2\pi} \int_{-\infty}^{\infty} \int_0^{\infty} \hat{s}(\omega) \omega^2 R_{pp}(\omega, p) J_0(\omega p r) \exp\{i\omega [q(2h-z)-t]\} p dp d\omega. \quad (3)$$

In the original reflectivity method, the slowness integral in equation (3) (a Hankel transform) is evaluated numerically for each frequency at a desired range r . This results in a frequency series which is inverse

Fourier transformed to give a time series, which when convolved with an appropriate source function yields the desired synthetic. If the order of the two transforms is interchanged, intermediate results are time series for particular values of slowness. These time series may be integrated numerically to give a time series at a particular distance. This alternate method is the slowness method.

THE SLOWNESS METHOD

We choose here to evaluate the Fourier transform in equation (3) before the Hankel transform. Changing the order of integration and applying the fundamental theorems of Fourier transformation (Bracewell 1965, p. 122), we get

$$w(r, z, t) = \frac{1}{r} \frac{d^2}{dt^2} \int_0^{\infty} \{s(t) * \check{J}_0(t/pr) * \check{R}_{pp}(t-q(2h-z), p)\} dp \quad (4)$$

where the star, *, denotes convolution in the time domain. \check{J}_0 and \check{R}_{pp} are the inverse Fourier transforms of the Bessel function J_0 and the reflectivity R_{pp} . Notice that while the original slowness integral of equation (2) involved a complex exponential and the complex function R_{pp} , the Fourier transformed version (equation 4) involves only real functions. The transformed reflectivity, \check{R}_{pp} , is real since the original function R_{pp} is Hermitian (i.e., $R_{pp}(\omega, p) = R_{pp}^*(-\omega, p)$). Hence, by Fourier transformation, the complex arithmetic of the original method has been eliminated and all subsequent computation involves only real quantities. However this does not imply that the slowness approach has any intrinsic computational superiority over the spectral approach; if the complex R_{pp} has been computed for $n/2$ frequencies, then the real \check{R}_{pp} is defined for n times, so the total

amount of computation required is identical in either method.

If the range r is large enough that the wavefronts are approximately planar, equation (4) can be simplified by using the far-field approximation for \check{J}_0 given by Chapman (1978),

$$\check{J}_0(t) = \frac{1}{2^{1/2}\pi} \left\{ \frac{H(1-t)}{(1-t)^{1/2}} + \frac{H(t+1)}{(t+1)^{1/2}} \right\},$$

where $H(t)$ is the Heaviside step function. Using this approximation,

$$\check{J}_0(t/pr) = \left(\frac{pr}{2} \right)^{1/2} \frac{1}{\pi} \left\{ \frac{H(pr-t)}{(pr-t)^{1/2}} + \frac{H(t+pr)}{(t+pr)^{1/2}} \right\}$$

The first term in parentheses represents a disturbance travelling with positive phase velocity; the second term, negative phase velocity. For body waves in the far field the second term will yield negligible contribution to the slowness integral. We ignore the second term and use

$$\check{J}_0(t/pr) = \left(\frac{pr}{2} \right)^{1/2} \frac{1}{\pi} \frac{H(pr-t)}{(pr-t)^{1/2}} \quad (5)$$

Substituting the approximation (5) into equation (4), readjusting time lags, and making use of the derivative of a convolution (Bracewell 1965, p. 118), we obtain

$$w(r,z,t) = \pi^{-1} (2r)^{-1/2} \ddot{s}(t) * \lambda(-t) * \int_0^\infty p^{1/2} \check{R}_{pp}(t-t_0,p) dp, \quad (6)$$

where, for convenience, we have defined the function $\lambda(t) = H(t)t^{-1/2}$ and where t_0 is the time delay

$$t_0 = pr + q(2h-z).$$

If $\lambda(t)$ is time-reversed it becomes its Hilbert transform, which we shall denote by an overbar, hence $\lambda(-t) = \overline{\lambda}(t)$. This Hilbert transformation can be moved to any convenient term in the convolutions of equation (6) since Hilbert-transformed convolutions have the property that

$$\overline{f*g} = \overline{f}*g = f*\overline{g}.$$

Since Hilbert transformation just involves changing the phase of spectral components, it is conveniently combined with Fourier transformation. We therefore choose to rewrite equation (6)

$$w(r,z,t) = \pi^{-1} (2r)^{-\frac{1}{2}} \ddot{s}(t) * \lambda(t) * \int_0^{\infty} p^{\frac{1}{2}} \overline{R}_{pp}(t-t_0, p) dp, \quad (7)$$

which has the same form as equation (30) of Chapman (1978).

At this point it is worth expanding on the meaning of \overline{R}_{pp} . The reflectivity $R_{pp}(\omega, p)$ is a plane wave function, as is readily apparent from equation (3). This means that for any particular slowness p , the inverse transform of R_{pp} , the time series $\overline{R}_{pp}(t, p)$, is the response of the structure to an impulsive plane wave of that slowness. Phinney *et al.* (1980) suggest that such time series be referred to as plane wave seismograms. We shall refer to the complete function \overline{R}_{pp} for all slowness as the plane wave response.

The original reflectivity function is computed without any consideration of source-receiver geometry. The Fourier transformation converts the frequency dependence to a time dependence, but the only time that can be

defined for the ocean bottom (or any surface) without specifying source and receiver separation is intercept time $\tau = t - pr$. Hence the time dependence of \check{R}_{pp} is intercept time at the ocean bottom. For the problem being considered, however, the source and receiver are not at the ocean bottom but some distance above it. As a result, the time argument of \check{R}_{pp} in equation (7) is not $t - pr$ but $t - pr - q(2h - z)$. The additional term $q(2h - z)$ is the total travel time of a disturbance in the water and must be subtracted to account for source-receiver geometry. If more than one layer were included in the region above the reflection zone, as in the original treatment of Fuchs & Müller (1971), additional time delay terms would appear in equation (7).

For many applications it is more convenient to work with angles rather than with slownesses. Let γ be the angle of incidence at the top of the reflection zone so that $\gamma = \sin^{-1}(p\alpha_0)$. Changing the variable of integration in equation (7) to γ leads to

$$w(r, z, t) = (2r\pi^2\alpha_0^3)^{-\frac{1}{2}} \ddot{s}(t) * \lambda(t) * \int_0^{\pi/2} \sin^{\frac{1}{2}}(\gamma) \cos(\gamma) \check{R}_{pp}(t - t_0, \gamma) d\gamma, \quad (8)$$

where the time delay t_0 is

$$t_0 = pr + q(2h - z) = \{r \sin\gamma + (2h - z) \cos\gamma\} / \alpha_0. \quad (9)$$

In equation (8) the integration has been limited to real angles of incidence. For body waves at sufficiently large range, truncating the integration at $\gamma = \pi/2$ leads to negligible error, but for surface waves or at close range the integration must be extended to complex angles of incidence (Stephen 1977).

Numerical Approach - A Simple Example

To compute synthetics using an expression of form similar to equation (7), Chapman (1978) suggests using the WKBJ approximation to solve the p integral. However, to retain generality and to compute synthetics for situations where the WKBJ approach is difficult to apply or is inappropriate, we choose to evaluate the integral numerically. The most obvious procedure is to compute the reflectivity function R_{pp} , transform to get \check{R}_{pp} , perform the p integrations at a series of times for a given range, and finally obtain a synthetic seismogram by convolving with the "effective source" $s(\check{t}) * \lambda(t)$. However, poorly defined D.C. levels and singularities in \check{R}_{pp} make the numerical integration rather noisy and unstable, so the obvious procedure has to be modified somewhat. The exact nature of such problems and the means of their solution are most readily explained using an example.

We shall consider the simple structure shown in Table 1 and describe how the slowness approach can be used to synthesize the vertical motion at the surface arising from a surface point source. The structure consists of a five kilometer deep homogeneous water layer, one kilometer of homogeneous sediments and an homogeneous basement. We choose to ignore the direct and surface-reflected phases, and to model only energy return from the ocean bottom. It is natural then to specify the top of the reflection zone as the water-sediment interface. The plane-wave reflectivity function R_{pp} for this structure was computed for frequencies from 0.0625 to 8 Hz and for angles from normal to grazing incidence on the bottom at increments of half a degree. This computation was performed using Fryer's (1978) modification of Kind's (1976) algorithm, although any equivalent procedure could have been used.

Table 1. A simple test model.

Layer Thickness (km)	P velocity (km/sec)	S velocity (km/sec)	Density	P wave Q	S wave Q
5.0	1.50	-	1.03	∞	-
1.0	2.0	1.0	1.7	200	20
∞	4.0	2.0	2.5	500	167

The modulus of the reflectivity function is shown in Fig. 2. The function is dominated by interference features. From normal incidence to 22° the interference fringes are primarily caused by compressional waves in the sediment. At 22° , compressional waves are critically incident at basement, resulting in a frequency-independent ridge. A similar ridge exists at 46° where compressional waves are critically reflected from the sediment and shear waves from the basement. Between these two angles is a complex region of interconversion and resonance. Beyond 46° , interference fringes arise from P-S conversion at the sediment-water interface and shear resonance within the sedimentary layer. The fringes decay rapidly with increasing frequency because of the low value (20) specified for shear wave Q .

THE INVERSE FOURIER TRANSFORM

If $R_{pp}(\omega, \gamma)$ is inverse Fourier transformed with respect to frequency we obtain the plane wave response $\overline{R}_{pp}(t, \gamma)$. Since the transform is of finite length, the usual problems of edge effects and side-lobes arise, so smoothing is necessary for the subsequent integration over angle to be stable. For this work smoothing was done in the frequency domain before transformation using a cosine-squared function tapering to zero at the Nyquist (although any gentle taper would have been adequate). In Chapman's WKBJ approach an equivalent smoothing is required (Dey-Sarkar & Chapman 1978). Part of the smoothed plane-wave response is plotted in Fig. 3. An explanation of those arrivals for which a simple ray interpretation is possible is shown in Fig. 4. In Fig. 4 each kinematic group is identified by the type and number of passages through the sediment layer; thus P^3S represents

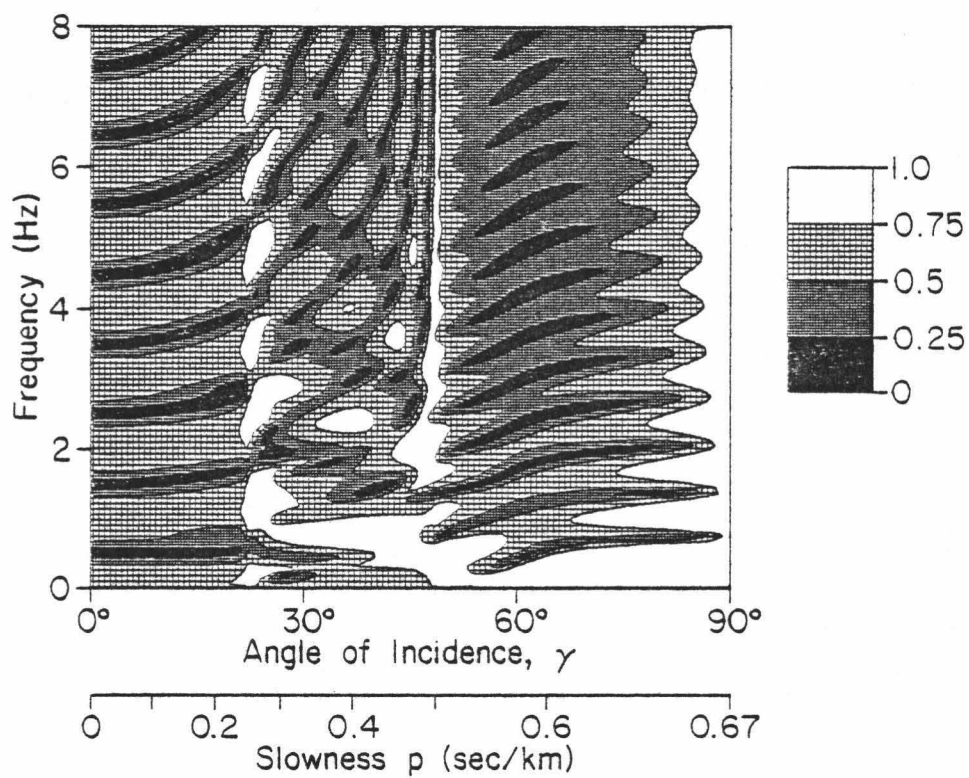


Figure 2. Modulus of the ocean bottom reflectivity function R_{pp} for the structure of Table 1.

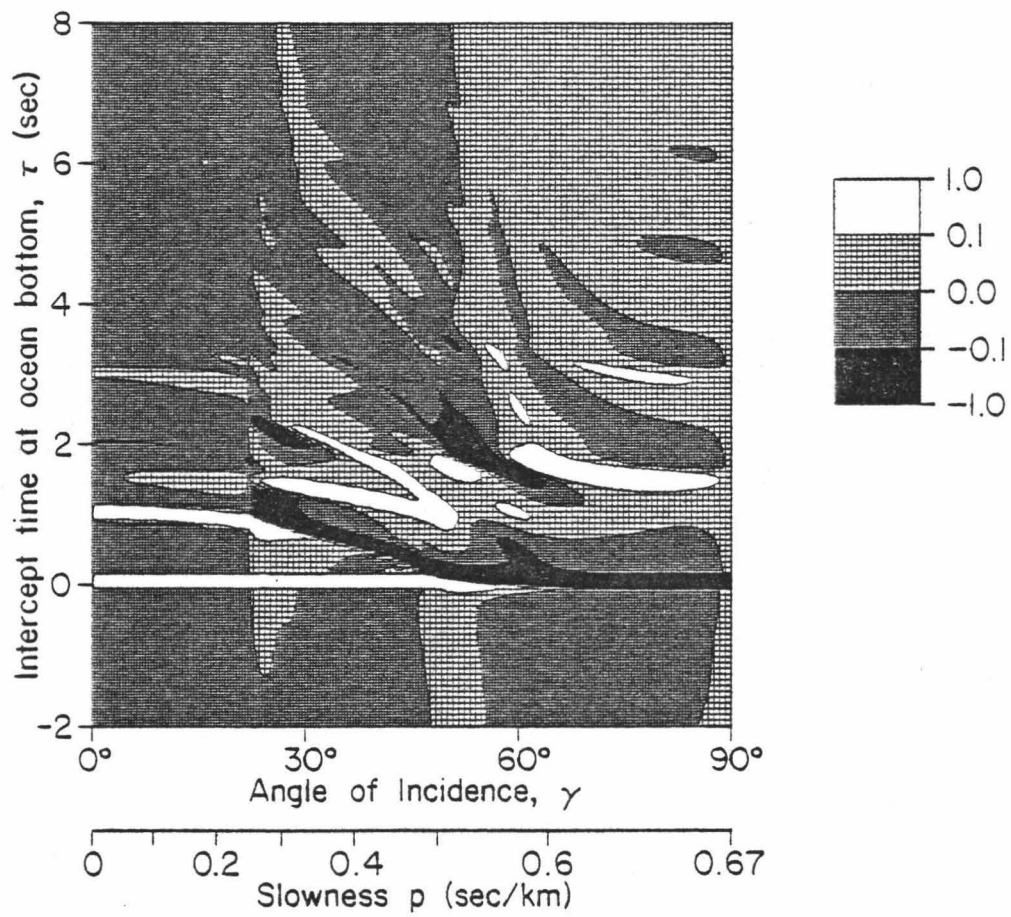


Figure 3. The plane wave response \tilde{R}_{pp} . Units are arbitrary.

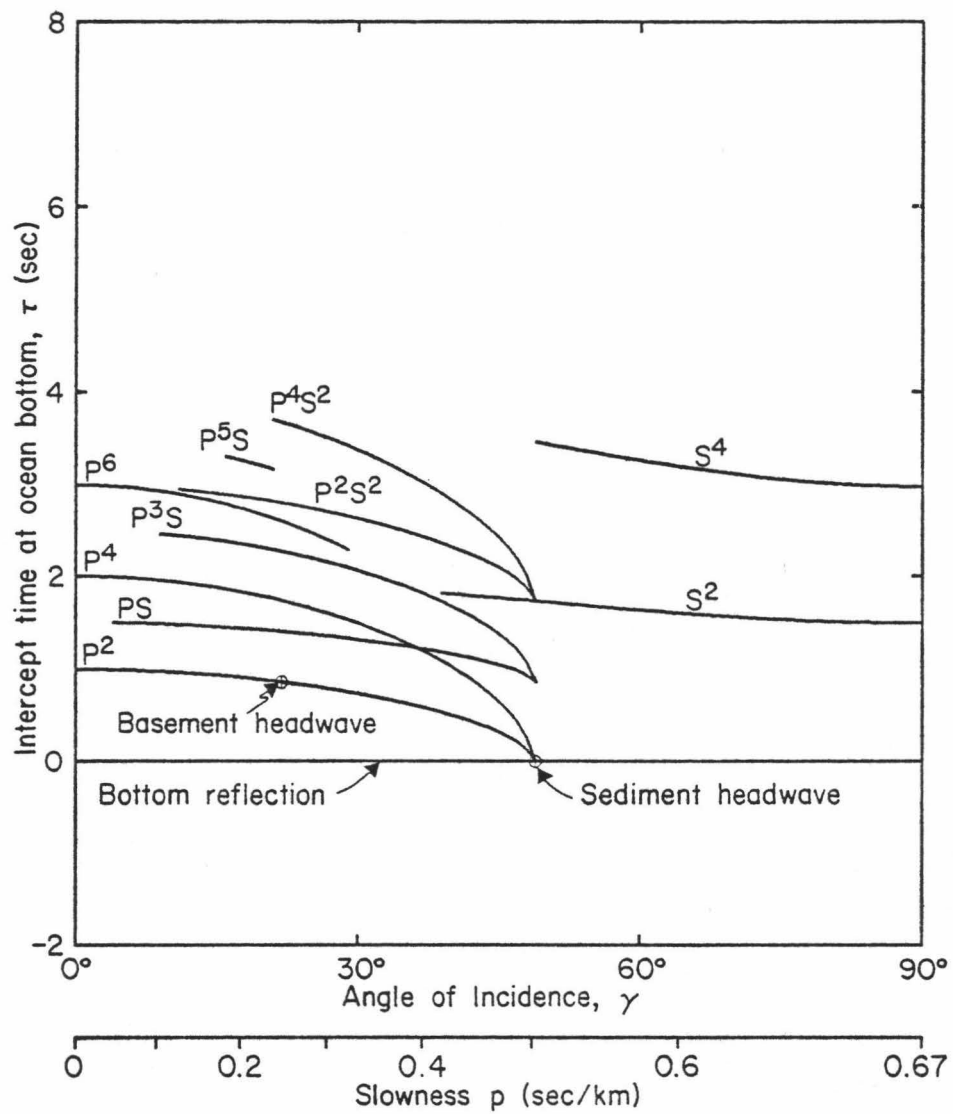


Figure 4. A ray interpretation of Fig. 3; see text for explanation.

all rays that make three passages as compressional waves and one passage as shear. The plane-wave response (Fig. 3) is as expected; first reflections are positive when they are subcritical, change rapidly in phase at the appropriate critical angle, and become negative for supercritical incidence. Multiples have the appropriate sign changes. In the vicinity of the critical angles at 22° and 46° , low amplitude precursors are apparent, these are a result of the phase change of arrivals near critical incidence, as described by Arons & Yennie (1950).

Since it is necessary for the plane wave response to be smoothed before further analysis, it is most economical to perform the convolution with the source function at the same time. The smoothing and convolution can be combined into a single step equivalent to convolution with a smoothed source function. It is a common practice to include the source by specifying the function $\dot{s}(t)$ (e.g. Fuchs & Müller 1971, Dey-Sarkar & Chapman 1978). This is because compressional wave displacement in the far-field is proportional to the derivative of the source displacement potential. For this example, the compressional wave displacement, and hence $\dot{s}(t)$, was chosen to be a simple half-sinusoid of half a second duration and the convolution-smoothing operation was performed by multiplication in the frequency domain. In this particular case the source function was sufficiently band-limited that the smoothing was probably unnecessary. The result of the convolution is shown isometrically in Fig. 5, a plot of $\dot{s}(t) * \bar{R}_{pp}(t, \gamma)$. Precursors at the critical angles are quite obvious in Fig. 5.

Because the reflectivity program used here could not compute zero frequency reflectivities, the lowest frequency used was 0.0625 Hz and zero frequency values were assumed to be zero. The time series obtained by inverse transformation of a frequency function with zero D.C. level must

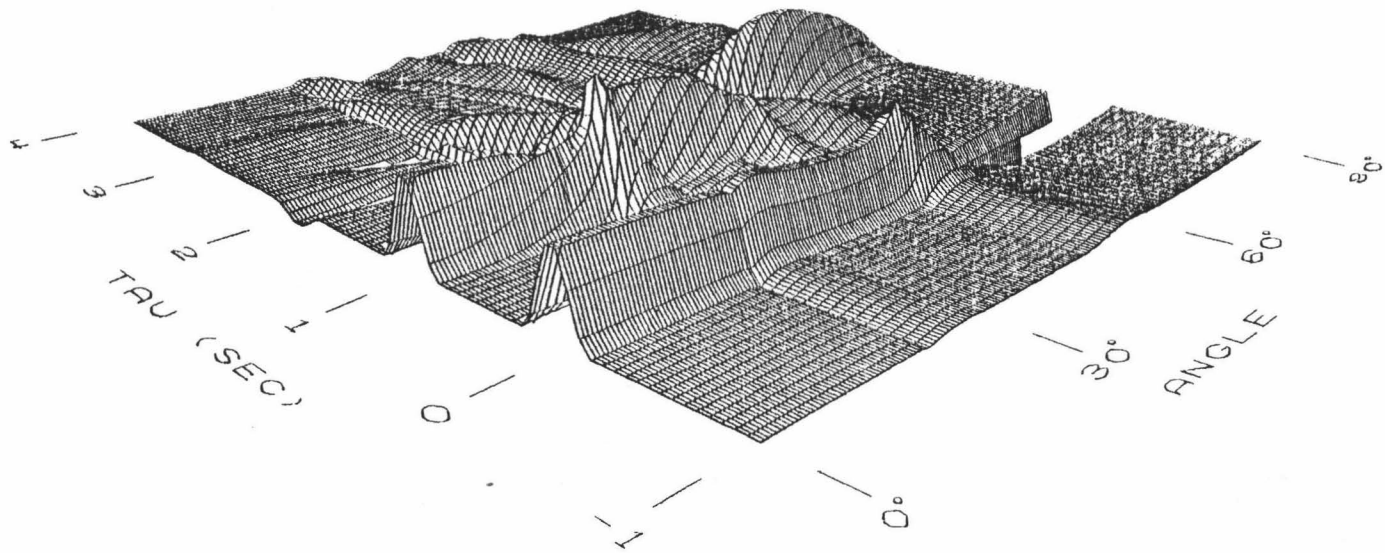


Figure 5. The plane wave response convolved with a half-sinusoid source function.

have a zero mean. However, a zero mean is likely to be inappropriate for a finite length time series as it may force the background level to be non-zero. For example, for the case considered here, the response near normal incidence is dominated by the positive bottom and basement reflections; since a zero D.C. level implies a zero mean, the whole of the rest of the response is mildly negative, as is apparent from 0 to 20° in Fig. 3. In any practical application of seismogram synthesis the lowest frequency used should not have to be any lower than the lowest frequency present in the source function, but ignoring lower frequencies can lead to slow, angle-dependent variation in the zero-level of the plane wave response. If the source function used does not have zero mean, this zero-level variation will introduce noise into the angle integration and give anomalous amplitudes for weak arrivals such as head waves. However, the problem is readily solved. Equation (8) shows that an additional time derivative is required in computing the synthetic. Since differentiation is a form of high-pass filtering, the zero offset is suppressed and the problem bypasses if the reflection response is differentiated before the angle integration.

As with the smoothing and source convolution operations, taking the derivative is most readily accomplished in the frequency domain before taking the initial transform (this is done simply by multiplying by $-i\omega$). We note from equation (10) that Hilbert transformation is also required, this is equivalent to multiplying the frequency function by $-i\text{sgn}(\omega)$. The two operations can obviously be combined by multiplying by $-|\omega|$. The final result is the function

$$W(t, \gamma) = \ddot{s}(t) * \bar{R}_{pp}(t, \gamma),$$

which is plotted in Fig. 6. It is apparent that despite the additional derivative, the surface W is smooth enough for the Hankel transformation to be evaluated by numerical integration. Note also that the "non-causal" precursors have been suppressed.

THE INVERSE HANKEL TRANSFORM

Once the function W of equation (10) has been obtained we wish to perform the inverse Hankel transformation by evaluating the angle integral from equation (8),

$$G(r,z,t) = \int_0^{\pi/2} \sin^{\frac{1}{2}} \gamma \cos \gamma W(t-t_0, \gamma) d\gamma \quad (11)$$

or the equivalent slowness integral from equation (7). The desired seismogram is then given by

$$w(r,z,t) = (2r\pi^2\alpha_0^3)^{-\frac{1}{2}} \lambda(t) * G(r,z,t). \quad (12)$$

The function $W(t, \gamma)$ is defined only on equally spaced grid points, so interpolation will be required to obtain values along the desired integration paths. Because source and receiver are not on the reflecting surface (the ocean bottom), the integration paths are not the straight lines that they are in Chapman's (1978) work, but follow curved trajectories across the W landscape. These curves are dependent on the source-receiver geometry and are defined by the delay time function $t_0 = t_0(r, z, \gamma)$ given in equation (9). For simplicity, for the rest of this paper, we shall assume that source and receiver are at the surface ($z=0$). For a 5 km deep ocean, t_0

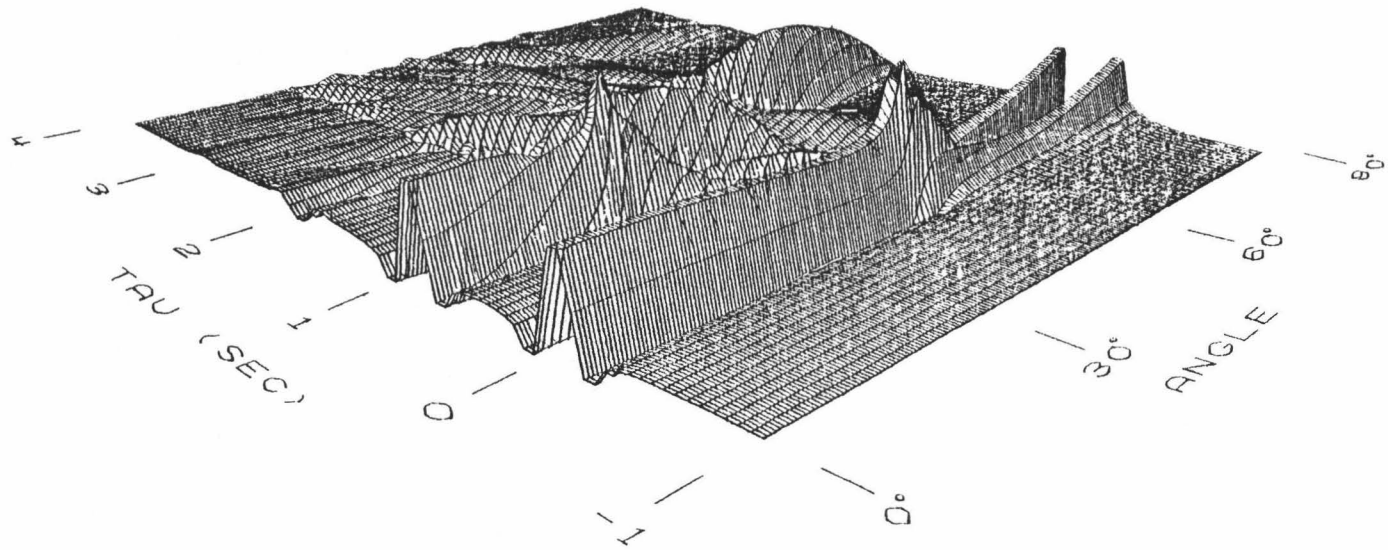


Figure 6. The function $W(t, \gamma)$ of Equation (10). This is the Hilbert transformed time derivative of Fig. 5.

then has the angle dependence shown in Fig. 7 for various values of range, r . For normal incidence the time delay is the vertical two-way travel time through the water layer, while its maximum for any range occurs at the appropriate angle for specular reflection off the ocean bottom. Hence, at a range of 10 km, t_0 is a maximum at 45° , the expected angle for a 5 km deep ocean.

To compute a synthetic for a particular range r' , the time series $G(r', 0, t)$ must be obtained by evaluating the integral (11) for the range of times of interest. The integral can be evaluated separately for each time, but this involves retrieval of information from the tabulated $W(t, \gamma)$ in a pseudo-transpose order and is extremely slow on a virtual memory computer. A better method is to consider the total contribution to $G(r', 0, t)$ for all times at a particular angle γ' , and then proceed to the next angle. This is done by computing $t_0(r', 0, \gamma')$, then linearly interpolating in time to obtain the series $W(t-t_0, \gamma')$ for the desired times $t=t_i$; $i=1, 2, 3, \dots, n$. Each term in this series is given the trigonometric weighting $\sin^{\frac{1}{2}} \gamma \cos \gamma$ and added to $G(r', 0, t_i)$; $i=1, 2, 3, \dots, n$, before proceeding to the next angle. If only half of the contribution from the limiting angles of the integration is taken, then this procedure amounts to a trapezoidal integration. As with the original reflectivity method (Fuchs & Müller 1971), the integration need include only that range of angles of interest in any problem.

The final step in computing seismograms is to perform the range-dependent weighting and convolution with $\lambda(t)$ shown in equation (12). Synthetics generated by using the rational approximation to $\lambda(t)$ given by Wiggins (1976) are shown in Fig. 8 with superposed travel times for the major phases. Wiggins' rational operator makes the convolution extremely rapid but is inaccurate for periods longer than about 100 times the sampling interval.

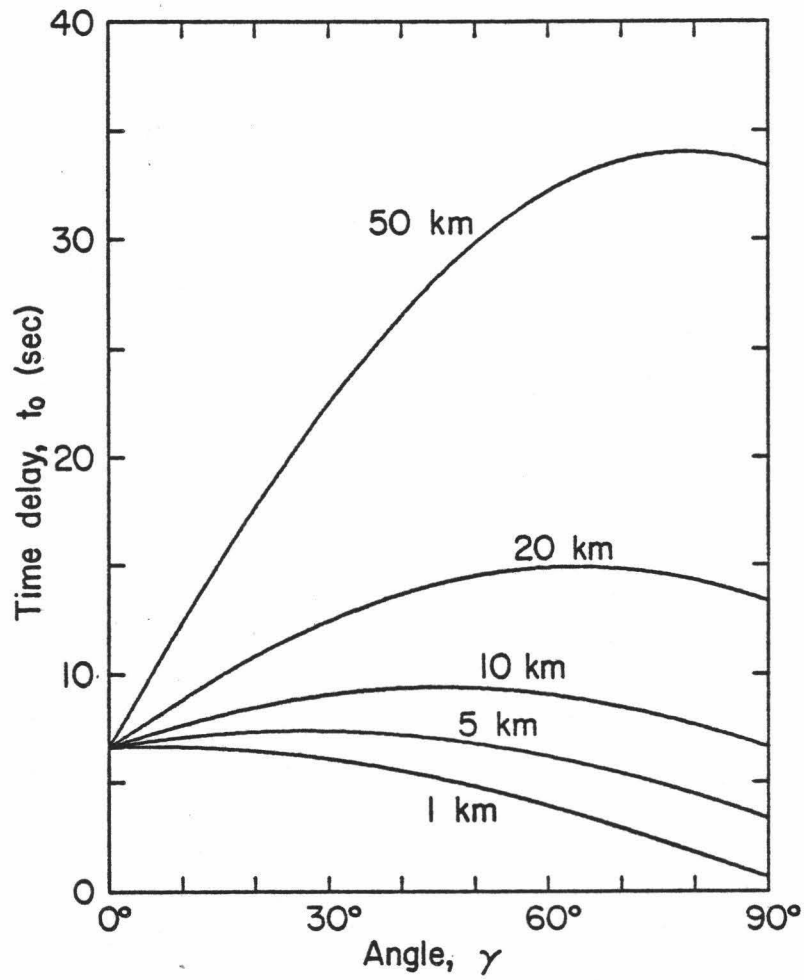


Figure 7. The time delay function t_0 for various ranges.

Such long-period errors are of no consequence to the short period seismograms plotted here. The synthetics shown in Fig. 8 are indistinguishable from those obtained from the original reflectivity method. The only difference is in computation time; after computation of the reflectivities, the original method took about four times longer than the slowness method.

Discussion

The reflectivity approach for computing synthetic seismograms is readily modified from a spectral to a slowness method. This modification was originally directed at reducing the expense of the reflectivity method, and indeed, considerable economies were realized. However, in retrospect, there is nothing in the mathematics which suggests the slowness method will be computationally superior. That the slowness approach was faster than the spectral is purely a consequence of superior code. The spectral program used, Kennett's (1975) modification of the original Fuchs & Müller (1971) program, has many options and broad application. Programs designed for specific problems always outperform general programs, and that is exactly what happened here.

Where the slowness approach does hold an advantage over the spectral is in the manner of construction of the seismograms. Reflectivity-slowness shares this advantage with another important slowness method, the WKBJ technique (Chapman 1978). The WKBJ method is much more economical than the reflectivity method but may be inappropriate for complicated structures with high gradients or low velocity zones. Both slowness methods allow us to visualize a seismogram as the integrated cross-section of the plane-wave response. As shown by Figs. 3 and 4, the plane-wave response is much more amenable to physical interpretation than the reflectivity function, so our

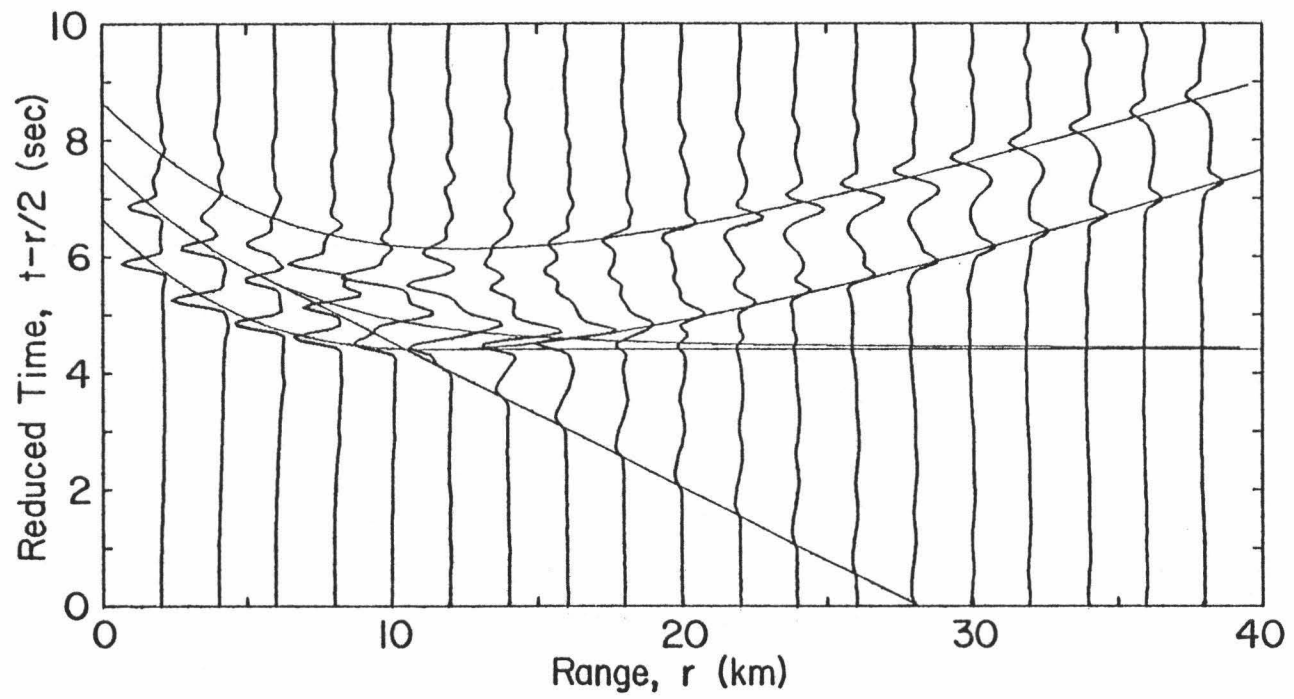


Figure 8. Seismograms and reduced travel times for the structure of Table 1.

physical comprehension of the synthesis process is improved. The plane wave response is also simpler to interpret than the final seismograms, as may readily be verified by comparing Figs. 3 and 8. For example, in τ - p space, reflections never cross in time and complications from interfering phases are greatly reduced. This would imply that it is better to analyse data and make comparison with models in τ - p space, a point which has important bearing on the inverse problem.

The most important recent advances in the inversion of seismic body wave data have come with the realization that travel time inversions are most effectively performed after transformation to τ - p space (Johnson & Gilbert 1972). This realization has resulted in a large number of inversion procedures for determining velocity-depth functions (e.g. Dorman 1979). However, such inversion schemes ignore amplitude information. The transformation of complete record sections to τ - p space seems a promising approach to an inversion scheme which would include an assessment of amplitudes (Phinney *et al.* 1980), although problems such as source deconvolution and the limitations of finite data density have yet to be resolved (Chapman 1978). Since the slowness approach involves computation of synthetics from τ - p space it again appears that that is the space in which to compare model and data. If the comparison could be quantified in some manner this would be an important step forward in the development of a practical solution to the inverse problem.

Acknowledgments

I thank George Sutton, Joe Gettrust and Neil Frazer for their critical comments. This study was supported by the Ocean Science and Technology Division of the Office of Naval Research.

This work forms part of a doctoral dissertation at the University of Hawaii. Hawaii Institute of Geophysics contribution number 0000.

References

- Arons, A.B., & Yennie, D.R., 1950. Phase distortion of acoustic pulses obliquely reflected from a medium of higher sound velocity, *J. acoust. Soc. Am.*, 22, 231-237.
- Bracewell, R., 1965. The Fourier transform and its applications, McGraw-Hill Book Company, New York.
- Burdick, L.J., & Orcutt, J.A., 1979. A comparison of the generalized ray and reflectivity methods of waveform synthesis, *Geophys. J. R. astr. Soc.*, 58, 261-278.
- Chapman, C.H., 1978. A new method for computing synthetic seismograms, *Geophys. J. R. astr. Soc.*, 54, 481-518.
- Dey-Sarkar, S.K., & Chapman, C.H., 1978. A simple method for the computation of body-wave seismograms, *Bull. seism. Soc. Am.*, 68, 1577-1593.
- Dorman, L.R., 1979. A linear relationship between Earth models and seismic body wave data, *Geophys. Res. Letters*, 6, 132-134.
- Fryer, G.J., 1978. Reflectivity of the ocean bottom at low frequency, *J. acoust. Soc. Am.*, 63, 35-42.
- Fuchs, K., & Müller, G., 1971. Computation of synthetic seismograms with the reflectivity method and comparison with observations, *Geophys. J. R. astr. Soc.*, 23, 417-433.
- Johnson, L.E., & Gilbert, F., 1972. Inversion and inference for teleseismic ray data, *Meth. comp. Phys.*, 12, 231-266, Academic Press, New York.
- Kennett, B.L.N., 1974. Reflections, rays and reverberations, *Bull. seism. Soc. Am.*, 64, 1685-1696.
- Kennett, B.L.N., 1975. Theoretical seismogram calculation for laterally varying crustal structures, *Geophys. J. R. astr. Soc.*, 42, 579-589.

- Kind, R., 1976. Computation of reflection coefficients for layered media, J. Geophys., 42, 191-200.
- Phinney, R. A., Chowdhury, K. R., & Frazer, L. N., 1980, Transformation and analysis of record sections, submitted to Geophys. J. R. astr. Soc.
- Stephen, R. A., 1977. Synthetic seismograms for the case of the receiver within the reflectivity zone, Geophys. J. R. astr. Soc., 51, 169-181.
- Wiggins, R. A., 1976. Body wave amplitude computations - II, Geophys. J. R. astr. Soc., 46, 1-10.